JCTC Journal of Chemical Theory and Computation

pubs.acs.org/JCTC Article

Low-Order Scaling G_0W_0 by Pair Atomic Density Fitting

Arno Förster* and Lucas Visscher

Cite This: J. Chem. Theory Comput. 2020, 16, 7381−7399

Read Online

ACCESS | Metrics & More | Article Recommendations | Supporting Information

ABSTRACT: We derive a low-scaling G_0W_0 algorithm for molecules using pair atomic density fitting (PADF) and an imaginary time representation of the Green's function and describe its implementation in the Slater type orbital (STO)-based Amsterdam density functional (ADF) electronic structure code. We demonstrate the scalability of our algorithm on a series of water clusters with up to 432 atoms and 7776 basis functions and observe asymptotic quadratic scaling with realistic threshold qualities controlling distance effects and basis sets of triple-ζ (TZ) plus double polarization quality. Also owing to a very small prefactor, a G_0W_0 calculation for the largest of these clusters takes only 240 CPU hours with these settings. We assess the accuracy of our algorithm for HOMO and LUMO energies in the GW100 database. With errors of 0.24 eV for HOMO energies on the quadruple-ζ level, our implementation is less accurate than canonical all-electron implementations using the larger def2-QZVP GTO-type basis set. Apart from basis set errors, this is related to the well-known shortcomings of the GW space-time method using analytical continuation techniques as well as to numerical issues of the PADF approach of accurately representing diffuse atomic orbital (AO) products. We speculate that these difficulties might be overcome by using optimized auxiliary fit sets with more diffuse functions of higher angular momenta. Despite these shortcomings, for subsets of medium and large molecules from the GW5000 database, the error of our approach using basis sets of TZ and augmented double-ζ (DZ) quality is decreasing with system size. On the augmented DZ level, we reproduce canonical, complete basis set limit extrapolated reference values with an accuracy of 80 meV on average for a set of 20 large organic molecules. We anticipate our algorithm, in its current form, to be very useful in the study of single-particle properties of large organic systems such as chromophores and acceptor molecules.

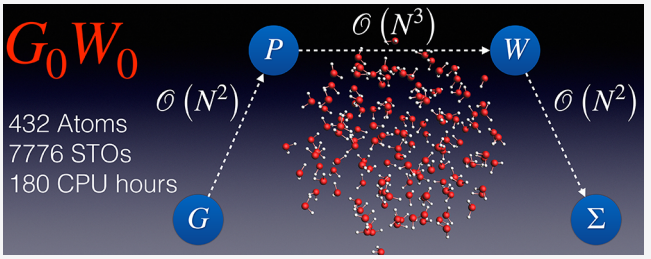

1. INTRODUCTION

Spectroscopy provides fundamental insights into the optical and electronic properties of matter and thus plays a decisive role in chemistry and material science.[1−5] The great potential of computational spectroscopy is leveraged increasingly to complement and understand spectroscopic experiments.[6−15] Still, no existing computational method can be applied routinely to systems of hundreds of atoms and simultaneously predict the outcome of a spectroscopic experiment with satisfactory accuracy.[15] For ground state properties, Kohn−Sham (KS)[16] density functional theory (DFT)[17−19] has been proven to be very accurate for many weakly correlated molecular systems.[20−26] Excited particles, however, interact strongly with other electrons and semilocal or hybrid approximations to the exact functional of KS-DFT do not capture this physics correctly.[27−36] Consequently, they fail to adequately describe single-particle excitations, which are necessary to understand and predict phenomena like transport,[37−39] tunneling,[40−42] or photoemission.[43−48]

The many body perturbation theory (MBPT)[49−51] based on Hedin's equations describes the correlation of the excited electron with its surrounding by an expansion in powers of the response of the system's total classical potential to an external perturbation.[52−54] In the GW approximation,[51,55] this expansion is truncated after first order, which accounts for the major part of electron correlation.[46,54,56,57] The GW approximation makes MBPT computationally tractable, greatly improves over DFT for the description of single-particle excitations,[46,53,58] and also paves the way toward accurate optical spectra using the Bethe-Salpeter equation formalism.[59,60] Large numbers of computational material science codes[48,56,61−72] feature GW implementations, and also in the quantum chemistry community, it has acquired some momentum over the last years.[58,73−93]

The downside of the GW method is its huge operation count compared to KS-DFT, preventing its routine application to large systems. A popular approach to reduce the prefactor, frequently outperforming self-consistent approaches for charged excitations,[58,94] is the so-called G_0W_0 approximation in which the self-energy is calculated using a mean-field Green's function. Still, the operation count of a G_0W_0

Received: July 3, 2020
Published: November 11, 2020

https://dx.doi.org/10.1021/acs.jctc.0c00693
J. Chem. Theory Comput. 2020, 16, 7381−7399

calculation increases as N^4 as a function[95] of system size N, and compared to KS-DFT, GW quasi-particle (QP) energies converge significantly slower with the size of the single-particle basis.[46,96,97] Consequently, the last years have witnessed some effort to reduce time-to-solution further, which resulted in massively parallel implementations optimized for state-of-the-art supercomputers[98,99] but also in notable algorithmic developments, including stochastic approaches,[100−102] implementations avoiding the explicit summation over empty electronic states in the polarizability, P[103−106] low-rank approximations to the dielectric function ϵ[64,97,107] or the screened interaction W,[108,109] and basis set error (BSE) correction schemes.[110−112]

In *ab initio* calculations on molecular systems, atom centered localized atomic orbitals (AOs) are commonly employed.[113] In this representation, the dimensions of W and P grow as N^2, making the evaluation of W an N^6 operation. One can employ an implicit low-rank approximation to both quantities by transforming them to a smaller auxiliary basis. Such transformations, most importantly density fitting (DF)[114−126] and Cholesky decomposition (CD)[127−131] techniques, have been employed in quantum chemistry for nearly half a century,[114−116] and they are routinely used in GW implementations for molecules[70,132−139] where their accuracy is well-documented.[82,135] Using these techniques, the evaluation of W becomes an N^3 operation with a sufficiently small prefactor. However, the transformations from the product basis to the auxiliary basis and back, usually implicit in the evaluation of P and the self-energy Σ, respectively, still scale as N^4.

This issue can in principle be avoided by constructing a sparse transformation matrix using local DF approximations (LDF).[140−143] However, conventional GW calculations are performed in frequency space, necessitating a representation of the Green's function in the MO basis where the sparsity of the transformation matrix is lost. From this perspective, the Green's function is more conveniently represented in imaginary time[29,144−148] since the energy denominator in P factorizes and the relevant equations can be transformed to the AO basis where LDF might be used efficiently.

LDF techniques have originally been proposed to evaluate the Fock matrix in generalized KS (gKS) and Hartree−Fock (HF) calculations in a low-scaling fashion.[115] This is fortunate since, in imaginary time, the evaluation of Σ is equivalent to calculating the exact exchange contribution to the Fock matrix. In the most extreme LDF variant, each AO-pair product is expanded in a set of auxiliary basis functions (ABF) centered on the same two atoms as the target pair of primitives. We refer to this approach as pair atomic density fitting (PADF) and note that also the names concentric DF, pair-atomic resolution of the identity (PARI), and RI-LVL are encountered in the literature. It was introduced by Baerends et al. in the 1970s[115] and subsequently employed in pure[149] and hybrid[140,150] DFT calculations. As an efficient way to construct the Fock matrix, it has received renewed attention over the last years[151−157] and its strengths and shortcomings for this task have been analyzed in detail.[158,159] It has also been applied to correlated methods and shown to be very accurate when appropriate auxiliary fit sets are used.[160−163]

For the GW space-time approach[147] to be useful in practice, small grids not only in imaginary time but also in imaginary frequency as well as an efficient way to switch between both domains are needed to avoid potentially prohibitive prefactors and storage bottlenecks. How to address these technical issues has been shown by Kresse and co-workers,[164,165] who subsequently presented cubic scaling GW implementations for periodic systems,[166,167] and also low-scaling space-time RPA[168,169] and GW[99] implementations for molecular systems have been realized in the last years.

It has already been anticipated[160] that PADF is especially well-suited to implement GW in a low-scaling fashion. Against this background, we herein derive a GW space-time algorithm whose asymptotic cost associated with the calculation of P and Σ is reduced to N^3, independent of system size, and to N^2 when distance effects are exploited. We only discuss our G_0W_0 implementation here while self-consistent GW will be discussed in a future publication. However, we stress that within the herein presented framework quasi-particle[170,171] and fully self-consistent GW is readily implemented as we always evaluate the complete self-energy matrix instead of only its diagonal in the MO basis.

We implemented our algorithm in the Slater type orbital (STO)-based Amsterdam density functional package (ADF).[172,173] Thus, our work is the first production level implementation of a GW method using STOs. While we do not aim at a comparison of different types of localized basis functions, we consider our implementation as a necessary first step toward a better understanding of the possible benefits of STOs in MBPT and also as a demonstration that they can be used efficiently in GW calculations. We also emphasize that the herein presented formalism is independent of the actual choice of basis functions, provided that they are local. We already note at this point that similar ideas have been presented by Wilhelm et al.[99] and implemented in the CP2K package.[48] We will start the following discussion in Section 2 by defining the basic quantities in real space (RS) and imaginary time, discretize them using an AO basis and imaginary time grids, and transform them to an auxiliary basis. From this starting point, we outline our algorithm and its implementation before we investigate its accuracy and computational efficiency in Section 3. Finally, Section 4 concludes this work with a summary and perspectives on further research.

2. THEORY

2.1. G_0W_0 in Real Space and Imaginary Time. We start this section by briefly outlining the G_0W_0 approximation to Hedin's equations in the random phase approximation (RPA).[53] Using the molecular orbitals ϕ_n and corresponding orbital energies ϵ_n obtained from solving

$$[h^{(0)}(\boldsymbol{r}) - \epsilon_n]\phi_n(\boldsymbol{r}) + \int_{\mathbb{R}^3} \mathrm{d}\boldsymbol{r}' V_{\mathrm{xc}}(\boldsymbol{r}, \boldsymbol{r}')\phi_n(\boldsymbol{r}') = 0 \tag{1}$$

with a single-particle Hamiltonian $h^{(0)}$ and a potentially local exchange-correlation (xc) potential V_{xc}, the irreducible single-particle time-ordered Green's function in imaginary time is given as

$$G(\boldsymbol{r}, \boldsymbol{r}', i\tau) = \Theta(\tau)\underline{G}(\boldsymbol{r}, \boldsymbol{r}', i\tau) - \Theta(-\tau)\overline{G}(\boldsymbol{r}, \boldsymbol{r}', i\tau) \tag{2}$$

with

$$\underline{G}(\boldsymbol{r}, \boldsymbol{r}', i\tau) = i\sum_{i}^{\mathrm{occ}} \phi_i(\boldsymbol{r})\phi_i^*(\boldsymbol{r}')e^{-|\epsilon_i - \epsilon_{\mathrm{F}}|\tau}$$

$$\overline{G}(\boldsymbol{r}, \boldsymbol{r}', i\tau) = i\sum_{a}^{\mathrm{virt}} \phi_a(\boldsymbol{r})\phi_a^*(\boldsymbol{r}')e^{|\epsilon_a - \epsilon_{\mathrm{F}}|\tau} \tag{3}$$

https://dx.doi.org/10.1021/acs.jctc.0c00693
J. Chem. Theory Comput. 2020, 16, 7381−7399

being the hole and particle Green's functions, respectively, i, j, ... (a, b, ...) labeling occupied (virtual) orbitals, ϵ_F being the Fermi energy, and Θ being the Heavyside step function. The independent-particle polarizability P in the RPA is defined as

$$P(\boldsymbol{r}, \boldsymbol{r}', i\tau) = -iG(\boldsymbol{r}, \boldsymbol{r}', i\tau)G(\boldsymbol{r}', \boldsymbol{r}, -i\tau) \tag{4}$$

and using (2) and (3) can be written as

$$P(\boldsymbol{r}, \boldsymbol{r}', i\tau) = -i \sum_{i}^{\text{occ}} \sum_{a}^{\text{virt}} \phi_i(\boldsymbol{r})\phi_i^*(\boldsymbol{r}')\phi_a(\boldsymbol{r}')\phi_a^*(\boldsymbol{r})e^{-|\epsilon_a-\epsilon_F|\tau}e^{-|\epsilon_i-\epsilon_F|\tau} \tag{5}$$

The polarizability is the kernel of a Dyson equation relating the reducible (or screened) Coulomb interaction $W(\boldsymbol{r}, \boldsymbol{r}', i\tau)$ to the bare Coulomb potential $V(\boldsymbol{r}, \boldsymbol{r}') = V'(\boldsymbol{r}, \boldsymbol{r}', i\tau)\delta(\tau - \tau')$ (see, e.g., ref 174 or 108)

$$W(\boldsymbol{r}, \boldsymbol{r}', i\tau - i\tau') = V(\boldsymbol{r}, \boldsymbol{r}') + \int \mathrm{d}\tau_4\, \mathrm{d}\boldsymbol{r}_3\, \mathrm{d}\boldsymbol{r}_4 V(\boldsymbol{r}, \boldsymbol{r}_3)P(\boldsymbol{r}_3, \boldsymbol{r}_4, i\tau - i\tau_4)W(\boldsymbol{r}_4, \boldsymbol{r}', i\tau_4 - i\tau') \tag{6}$$

which takes the simpler form[148]

$$W^{-1}(\boldsymbol{r}, \boldsymbol{r}', i\omega) = V^{-1}(\boldsymbol{r}, \boldsymbol{r}') - P(\boldsymbol{r}, \boldsymbol{r}', i\omega) \tag{7}$$

in the imaginary frequency domain. From this quantity, the irreducible self-energy Σ can be constructed,[53] which is most conveniently split into a static and a dynamic contribution, $\Sigma = \Sigma^x + \Sigma^c$. The former is the HF exchange kernel and is given as

$$\Sigma^x(\boldsymbol{r}, \boldsymbol{r}') = i\underline{G}(\boldsymbol{r}, \boldsymbol{r}', i\tau = 0)V(\boldsymbol{r}, \boldsymbol{r}') \tag{8}$$

and the latter is given as

$$\Sigma^c(\boldsymbol{r}, \boldsymbol{r}', i\tau) = iG(\boldsymbol{r}, \boldsymbol{r}', i\tau)\tilde{W}(\boldsymbol{r}, \boldsymbol{r}', i\tau) \tag{9}$$

where we have introduced $\tilde{W} = W - V$. In a self-consistent procedure, G would be updated by solving another Dyson equation containing Σ as its kernel. In a G_0W_0 calculation, Σ^c is transformed to the imaginary frequency axis from where it is analytically continued to the complex plane.[175,176] The QP energy ϵ_n^{QS} is the ω which fulfills

$$0 = \omega - \epsilon_n - \langle n|Re(\Sigma^c(\omega)) + \Sigma_x - V_{xc}|n\rangle \tag{10}$$

where $\langle n|O|m\rangle$ denotes the matrix elements of an operator O in the molecular orbital basis.

2.2. G_0W_0 in a Local Basis. *2.2.1. Discretization of Real Space.* Assuming we have represented the imaginary time and frequency dependence of all quantities through suitable grids, we use a set of real STOs $\{\chi\}$ to discretize RS so that

$$\phi_n(\boldsymbol{r}) = \sum_{\mu} b_{\mu n}\chi_\mu(\boldsymbol{r}) \tag{11}$$

The insertion of this definition into eqs 2 and 3 gives

$$\underline{G}(\boldsymbol{r}, \boldsymbol{r}', i\tau) = \sum_{i} \sum_{\mu\nu} \chi_\mu(\boldsymbol{r})b_{\mu i}e^{-|\epsilon_i-\epsilon_F|\tau}b_{i\nu}\chi_\nu(\boldsymbol{r}') \tag{12}$$

$$\bar{G}(\boldsymbol{r}, \boldsymbol{r}', i\tau) = \sum_{a} \sum_{\mu\nu} \chi_\mu(\boldsymbol{r})b_{\mu a}e^{|\epsilon_a-\epsilon_F|\tau}b_{a\nu}\chi_\nu(\boldsymbol{r}') \tag{13}$$

and from the identity

$$G(\boldsymbol{r}, \boldsymbol{r}', i\tau) = \sum_{\mu\nu} \chi_\mu(\boldsymbol{r})G_{\mu\nu,\tau}\chi_\nu(\boldsymbol{r}') \tag{14}$$

we obtain the representation of the particle and hole Green's function in the STO basis

$$\underline{G}_{\mu\nu,\tau} = \sum_{i} b_{\mu i}e^{-|\epsilon_i-\epsilon_F|\tau}b_{i\nu} \tag{15}$$

$$\bar{G}_{\mu\nu,\tau} = \sum_{a} b_{\mu a}e^{|\epsilon_a-\epsilon_F|\tau}b_{a\nu} \tag{16}$$

which for each discrete $i\tau$ can be seen as an energy-weighted density matrix.[177] While Σ also transforms as a 2-point correlation function,

$$\Sigma_{\mu\nu,\tau} = \int \mathrm{d}\boldsymbol{r}\, \mathrm{d}\boldsymbol{r}'\chi_\mu(\boldsymbol{r})\Sigma(\boldsymbol{r}, \boldsymbol{r}', i\tau)\chi_\nu(\boldsymbol{r}') \tag{17}$$

all 2-electron operators transform as 4-point correlation functions,[178]

$$P_{\mu\kappa\nu\lambda,\tau} = i\underline{G}_{\mu\nu,\tau}\bar{G}_{\kappa\lambda,\tau} \tag{18}$$

$$V_{\mu\nu\kappa\lambda} = \int \mathrm{d}\boldsymbol{r}\, \mathrm{d}\boldsymbol{r}'\chi_\mu(\boldsymbol{r})\chi_\nu(\boldsymbol{r})V(\boldsymbol{r}, \boldsymbol{r}')\chi_\kappa(\boldsymbol{r}')\chi_\lambda(\boldsymbol{r}') \tag{19}$$

$$\tilde{W}_{\mu\nu\kappa\lambda,\tau} = \int \mathrm{d}\boldsymbol{r}\, \mathrm{d}\boldsymbol{r}'\chi_\mu(\boldsymbol{r})\chi_\nu(\boldsymbol{r})\tilde{W}(\boldsymbol{r}, \boldsymbol{r}', i\tau)\chi_\kappa(\boldsymbol{r}')\chi_\lambda(\boldsymbol{r}') \tag{20}$$

The calculation of the screened interaction (20) using P and V requires the inversion of a matrix in the AO product space $\mathcal{P} = \{\chi_\mu\} \otimes \{\chi_\nu\}$ for all frequency points (either of W^{-1} as in (7) or of the dielectric function ϵ, which is calculated from P and V) whose dimension scales as N^2 with the system size. Hence, the matrix inversion scales as N^6.

This scaling does not reflect the systems physics and is simply an artifact of the chosen representation. The Eckard−Young theorem guarantees the optimal rank-r approximation $M^{(r)}$ to some matrix M to be given by the first r terms in the sum on the *r.h.s.* of

$$M^{(r)} = \sum_{i}^{r} \sigma_i v_i \otimes u_i, \qquad \sigma_i \geq \sigma_{i+1} \tag{21}$$

where σ is a singular value and v_i and u_i are vectors of the matrices V and U from the singular value decomposition (SVD) of M. In this way, one can indeed show that the ranks of P, V, and W should only grow linearly with the system size[179] and using (21) one might decompose P, V, and W (given that they are symmetric) as

$$M_{\mu\nu\kappa\lambda} = \sum_{pq} C_{\mu\nu p}Z_{pq}[C^T]_{q\kappa\lambda}, \qquad M = P, V, \tilde{W} \tag{22}$$

where Z is the diagonal matrix of singular values and C collects the left singular vectors of M. An explicit SVD would scale as $N_{AO}{}^4 r$ and is prohibitive in practice.[179] Instead, it is common practice to represent V and W in a predefined auxiliary basis $\mathcal{A} = \{f\}$, whose size is growing linearly with the system size. Expanding all AO-pair products in terms of $\mathcal{A}$,

$$\chi_\mu(\boldsymbol{r})\chi_\nu(\boldsymbol{r}) = \sum_{p} C_{\mu\nu p}f_p(\boldsymbol{r}) \tag{23}$$

where Greek lowercase letters label AOs and the Roman lowercase letters p, q, ... refer to ABFs, V and $\tilde{W}$ can be expressed as

$$V_{pq} = \int \mathrm{d}\boldsymbol{r}\, \mathrm{d}\boldsymbol{r}' f_p(\boldsymbol{r})V(\boldsymbol{r}, \boldsymbol{r}')f_q(\boldsymbol{r}') \tag{24}$$

https://dx.doi.org/10.1021/acs.jctc.0c00693
J. Chem. Theory Comput. 2020, 16, 7381−7399

$$\tilde{W}_{pq} = \int \mathrm{d}\boldsymbol{r}\,\mathrm{d}\boldsymbol{r}' f_p(\boldsymbol{r})\tilde{W}(\boldsymbol{r},\boldsymbol{r}')f_q(\boldsymbol{r}') \tag{25}$$

and with (22) and (23), the equations to be solved in a G_0W_0 calculation become

$$P_{pq,\tau} = C_{\mu\nu p}P_{\mu\nu\kappa\lambda,\tau}C_{\kappa\lambda q} = -iC_{\mu\nu p}\underline{G}_{\mu\kappa,\tau}\bar{G}_{\nu\lambda,\tau}C_{\kappa\lambda q} \tag{26}$$

$$W_{pq,\omega} = V_{pq} + V_{pr}P_{rs,\omega}W_{sq,\omega} = [V^{-1} - P]^{-1}_{pq,\omega} \tag{27}$$

$$\Sigma^x_{\mu\nu} = i\sum_{\kappa\lambda}\sum_{pq}\underline{G}_{\kappa\lambda,\tau=0}C_{\mu\kappa q}V_{pq}C_{\nu\lambda p} \tag{28}$$

$$\Sigma^c_{\mu\nu,\tau} = i\sum_{\kappa\lambda}\sum_{pq}G_{\kappa\lambda,\tau}C_{\mu\kappa q}\tilde{W}_{pq,\tau}C_{\nu\lambda q} \tag{29}$$

replacing eqs 5 and 7−9. In this set of equations, (26) is the computational bottleneck. While the basis transformation in the first equation (26) would scale as N^5, also using the second equation one (27) ends up with a scaling of N^4. The same is actually true for (8) and (9); however, since in a G_0W_0 calculation only the diagonal elements of Σ in the MO basis are needed, the computational effort reduces to N^3.

Improvements over the N^4 scaling can be achieved in essentially two ways. The first way relies on the asymptotically exponential decay of the density matrix.[180−182] Ochsenfeld and co-workers exploited the resulting sparsity in $\underline{G}$ and $\bar{G}$[183] to calculate correlation energies in the second-order Møller−Plesset perturbation theory (MP2)[184−186] and RPA.[187−190] It is an obvious drawback of the approach that in 3D systems the density matrix is less sparse as one would hope for,[191−193] especially for large AO basis sets with many diffuse functions, which are commonly employed in GW calculations. The second way is to construct a sparse map from $\mathcal{P}$ to $\mathcal{A}$. How this can be achieved will be discussed in the next paragraph.

2.2.2. Local Density Fitting Approximations. Given some target precision ϵ, the two main goals of DF are first to find a matrix M' with dimension N_{aux} for which

$$\|M - M'\| < \epsilon \tag{30}$$

with N_{aux} as small as possible and M defined by (22) and second to improve over the unfavorable scaling of eqs 26, 28, and 29 by constructing C in a way that it becomes sparse. Both goals are in principle in conflict with each other. In DF, one minimizes the residual function

$$r_{\mu\nu}(\boldsymbol{r}) = \chi_\mu(\boldsymbol{r})\chi_\nu(\boldsymbol{r}) - \sum_p C_{\mu\nu p}f_p(\boldsymbol{r})\ \forall\ \mu,\nu \tag{31}$$

with respect to some appropriate norm. In the RI-V approach, the Coulomb repulsion of r is minimized,

$$\frac{\partial}{\partial C_{\kappa\lambda q}}\int \mathrm{d}\boldsymbol{r}\,\mathrm{d}\boldsymbol{r}' r_{\kappa\lambda}(\boldsymbol{r})V(\boldsymbol{r},\boldsymbol{r}')r_{\mu\nu}(\boldsymbol{r}') = 0 \tag{32}$$

and it follows that

$$\sum_p C_{\mu\nu p}V_{pq} = \int \mathrm{d}\boldsymbol{r}\,\mathrm{d}\boldsymbol{r}'\chi_\mu(\boldsymbol{r})\chi_\nu(\boldsymbol{r})V(\boldsymbol{r},\boldsymbol{r}')f_q(\boldsymbol{r}') \tag{33}$$

I.e., the error in the low-rank approximation of V is quadratic in r since the terms linear in C vanish. Of course, a similar conclusion can not be drawn for P and consequently also not for W. Still, it seems that this metric is an excellent choice if the goal is to fulfill (30) with N_{aux} as small as possible and use auxiliary fit sets from standard libraries. As shown by van Setten et al., QP HOMOs and LUMOs only deviate by a few meV from the ones obtained from the calculations without any low-rank approximation[82,135] when appropriate auxiliary fit sets[125,194] are used.

On the other hand, RI-V is a very bad choice in the sense that the slow decay of the kernel of the Coulomb operator ensures that C will be dense. In the RI-SVS approach,[118,121] (31) is minimized with respect to the L_2 norm, which requires larger N_{aux} to fulfill (30) but results in a C with the number of nonzero elements increasing only linearly with the system size for exponentially decaying basis functions. It has been shown by Wilhelm et al. that this approach results in tremendous speedups in the evaluation of eqs 26, 28, and 29 without requiring too large of an N_{aux} to make the evaluation of (27) problematic for systems of more than 1000 atoms.[99] However, for rather small systems with a 3D structure, the number of nonzero elements in C will not be much different from $N_{AO}^2 \times N_{\mathrm{aux}}$. Thus, due to the usually larger N_{aux} compared to RI-V, the method will only be advantageous for sufficiently large systems.[99]

In LDF approximations, this shortcoming is addressed by building in sparsity into the fitting procedure *a priori*. In PADF, an expansion of the pair-density $\chi_\mu(\boldsymbol{r})\chi_\nu(\boldsymbol{r})$ of the form

$$\chi_\mu(\boldsymbol{r})\chi_\nu(\boldsymbol{r}) = \sum_{p\in A\cup B}C_{\mu\nu p}f_p(\boldsymbol{r})\ \forall\ \mu\in A,\nu\in B \tag{34}$$

is employed so that the number of nonzero elements in C scales at the most quadratic with the system size. In our implementation, we also define thresholds $d_{\mu\nu}$ for each AO product and assume $C_{\mu\nu p} = 0$ if $|\boldsymbol{R}_A - \boldsymbol{R}_B| > d_{\mu\nu}$ so that the number of nonzero elements in C only increases linearly.[162] For each atom, we also reorder all AOs from the most diffuse to the least diffuse one so that all nonzero elements in C are grouped in dense blocks. Equation 31 becomes

$$r^{\mathrm{PADF}}_{\mu\nu}(\boldsymbol{r}) = \chi_\mu(\boldsymbol{r})\chi_\nu(\boldsymbol{r}) - \sum_{p\in A\cup B}C_{\mu\nu p}f_p(\boldsymbol{r})\ \forall\ \mu\in A,\nu\in B \tag{35}$$

which is minimized with respect to the Coulomb metric. Solving

$$\frac{\partial}{\partial C_{\kappa\lambda q}}\int \mathrm{d}\boldsymbol{r}\,\mathrm{d}\boldsymbol{r}' r^{\mathrm{PADF}}_{\kappa\lambda}(\boldsymbol{r})V(\boldsymbol{r},\boldsymbol{r}')r^{\mathrm{PADF}}_{\mu\nu}(\boldsymbol{r}') = 0 \tag{36}$$

does not lead to an equation of the form (33) as the terms linear in C do not vanish. Thus, determining C by solving (33) for all (nearby) atom pairs (A, B) leads to errors for V linear in r (the same holds for DF in the RI-SVS approach). It has been concluded that the resulting errors are too large for the method to be useful in HF calculations.[123,124,156] This might be true when standard auxiliary fit sets are used, which are optimized for global DF. In principle, the error of the expansion (23) can always be made arbitrarily small when an appropriate fit set is used although this is highly nontrivial. Simply increasing the number of ABFs does not always result in reduced errors and might even lead to numerical instabilities in the fitting procedure due to an increase of the linear dependencies in the auxiliary basis set.[162]

Another difficulty arises from the presence of diffuse functions in the AO basis set. To understand the source of the problem, we recall that very large AO basis sets with many diffuse functions might be locally overcomplete, which causes an almost linear dependence of a subset of basis functions.

https://dx.doi.org/10.1021/acs.jctc.0c00693
J. Chem. Theory Comput. 2020, 16, 7381−7399

These lead to numerical instabilities in the SCF[195] during canonical orthonormalization when the condition number of the AO-overlap matrix approaches infinity.[196] To restore numerical stability, one projects out the almost linearly dependent part from the basis by removing eigenvectors from the transformation matrix corresponding to eigenvalues of the AO-overlap matrix that are smaller than some threshold ϵ_D,[197] effectively diminishing the basis set size. This is not a severe restriction in practice since numerical instabilities usually do not occur when all eigenvalues are larger than $\epsilon_D = 10^{-6}-10^{-7}$.[198−200]

Using PADF, numerical instabilities can already occur when all eigenvalues are considerably larger as has, e.g., been observed for linear-response TDDFT with augmented basis sets[201] and MP2/QZ calculations.[162] The reason for this behavior is that individual fitting coefficients can become quite large for diffuse products from AOs centered on distant atoms. Note that this is a fundamental difference to global DF. As a qualitative example, consider a linear alkane chain C_nH_{2n+2} and the pair product of diffuse AOs on C_1 and C_n, respectively. The AOs will only have some (small) overlap in the middle of the chain. In global DF, this pair product could possibly be described very well with only a small set of ABFs centered on atoms in this region. In PADF, this overlap needs to be described with the asymptotic tails of diffuse ABFs on C_1 and C_n. When there is no appropriate ABF in the auxiliary basis, this will lead to very large fitting coefficients for some (diffuse) ABFs. In the transformation of the Coulomb potential from the auxiliary basis to the AO product basis, these large fitting coefficients must cancel with contributions with an opposite sign, which is numerically unstable.[202] Thus, relatively small errors might accumulate during the SCF and lead to an erroneous (hole) density matrix and potentially wrong eigenvalues.

To summarize, projecting out parts of the basis during canonical orthonormalization plays a dual role when PADF is used in the SCF. First, it ensures numerical stability of the SCF, and second, as a side-effect, it removes the part of the basis that potentially results in diffuse AO products, which are potentially difficult to fit. This nicely illustrates that the appropriate choice of the auxiliary basis and the problem of linear dependencies are intertwined. The addition of more diffuse functions to the auxiliary basis pair product in our example can be better approximated; the fitting coefficients become smaller, and the linear dependency problem is extenuated. This means the number of AOs that need to be removed becomes smaller and larger basis sets can be used in practice.

In the present work, we employ auxiliary fit sets that have been optimized for gKS calculations with PADF. Using these fit sets, we have shown recently[162,163] that the accuracy of PADF-MP2 is similar to global DF-MP2 with GTOs for basis sets of up to triple-ζ (TZ) quality. On the other hand, using quadruple-ζ (QZ) and also smaller basis sets augmented with diffuse functions sometimes result in unreliable PADF-MP2 ground state energies. It is clear that the same issues will arise in *GW* calculations.

For correlated methods, we observed that a value of $\epsilon_D = 10^{-3}$, corresponding to a drastic truncation of the basis, seems to provide a good trade-off between accuracy and numerical stability for all basis sets beyond TZ quality and also augmented basis sets. However, while this truncation prevents collapse to artificially low QP energies, it also leads to deteriorated results compared to the default of $\epsilon = 10^{-4}$. When the basis set is increased more and more, larger and larger parts of the virtual space need to be projected out, which ultimately prevents us from reaching the complete basis set (CBS) limit for the correlated methods. We expect, however, that carefully optimized auxiliary fit sets will enable the numerically stable application of PADF to these methods with larger basis sets. Before we discuss the accuracy of the present approach in Section 3, we will describe in some detail how PADF can be used to implement eqs 26−29 efficiently.

2.3. GW Equations with Pair Atomic Density Fitting.

In this section, we outline how the sparsity of the map from $\mathcal{P}$ to $\mathcal{A}$ can be exploited to implement GW in a low-scaling fashion.

2.3.1. Imaginary Time and Frequency Grids. After the calculation of the Coulomb potential and its inverse in the basis of ABFs and the basis transformation matrix C as described in Section 2.2, we calculate imaginary frequency and imaginary time grids, $\{\omega_k\}_{k=1,\ldots N_\omega}$, $\{\tau_k\}_{k=1,\ldots N_\tau}$, respectively. As outlined by Kresse and co-workers,[164] they can be evaluated by minimizing either the L_∞ (Chebyshev) or L_2 norm of

$$\eta(\{\alpha,\beta\},x) = \frac{1}{x} - f(\{\alpha,\beta\},x),$$
$$f = \begin{cases} 2\sum_{k=1}^{N_\tau} \alpha_k e^{-\beta_k x} & \beta = \tau \\ \frac{1}{\pi}\sum_{k=1}^{N_\omega} \alpha_k \frac{2x}{x^2+\beta_k^2} & \beta = \omega \end{cases} \tag{37}$$

with respect to the parameter sets α, β, where $x \in [\epsilon_{min}, \epsilon_{max}]$, where ϵ_{min} (ϵ_{max}) denotes the smallest (largest) KS orbital energy difference. Imaginary time and imaginary frequency domains are connected through Laplace transforms (see also Cancés et al.[175])

$$f(i\tau) = \frac{i}{2\pi}\int d\omega f(i\omega)(\cos(\omega\tau) + i\sin(\omega\tau)) \tag{38}$$

$$f(i\omega) = -i\int d\tau f(i\tau)(\cos(\omega\tau) - i\sin(\omega\tau)) \tag{39}$$

For our purpose, it is sufficient to treat them as Fourier transforms. To avoid potentially inaccurate interpolation to equidistant grids in order to use discrete Fourier transforms, we discretize (39) as

$$f(i\omega_k) = -i\sum_j^{N_\tau} \{\gamma_{kj}^{(c)}\cos(\omega_k\tau_j)(f(i\tau_j) + f(-i\tau_j)) - i\gamma_{kj}^{(s)}\sin(\omega_k\tau_j)(f(i\tau_j) - f(-i\tau_j))\} \tag{40}$$

where the weights $\gamma_{kj}^{(c)}$ and $\gamma_{kj}^{(s)}$ account for the nonuniformity of the grids. They are chosen to minimize the L_2 norm of the error introduced by (40) for $f(i\tau) = e^{-x|\tau|}$, $x \in [\epsilon_{min}, \epsilon_{max}]$ with respect to the exact transformation eq 39. By inverting the matrices $\gamma_{kj}^{(c)}\cos(\omega_k\tau_j)$ and $\gamma_{kj}^{(s)}\sin(\omega_k\tau_j)$, respectively, one can use the same relation to transform f from the imaginary frequency to imaginary time. To calculate the imaginary time grid, we minimize the L_∞ norm of (37) as implemented by Helmich-Paris et al.,[203,204] and in imaginary frequency, we minimize the L_2 norm on a logarithmic grid using a Levenberg−Marquardt algorithm.[205,206] Both algorithms require pretabulated values to converge to an acceptable local

https://dx.doi.org/10.1021/acs.jctc.0c00693
J. Chem. Theory Comput. 2020, 16, 7381−7399

minimum. For the imaginary time domain, we use the values distributed with the source-code of Helmich-Paris et al.,[207] and for the imaginary frequency domain, we tabulated our own values that we include in the Supporting Information.

2.3.2. Polarizability. After the Green's function [(15) and (16)] has been constructed, P can be evaluated. In this section, we use μ, ν, κ, and λ to denote AOs and α, β, γ, and δ to denote ABFs and the convention that $(\mu, \alpha) \in A$, $(\nu, \beta) \in B$, $(\kappa, \gamma) \in C$, and $(\lambda, \delta) \in D$, where A, B, C, and D label atoms. We denote the three-leg tensor collecting all fitting coefficients corresponding to all products formed from AOs centered on A and B and to ABFs centered on B as C^{ABB}, i.e., C^{ABB} contains only coefficients corresponding to fit functions centered on B. Consequently, the fitting coefficient tensor corresponding to all products formed from AOs on A and B and to ABFs centered on A and B is split into $C^{ABB} + C^{BAA}$. We also define $C^{ABB} = \frac{1}{1+\delta_{AB}}\tilde{C}^{ABB}$ to avoid complications from double counting. The contribution of each atom pair (A, B) to P, eq 26, is given as the sum of four contributions

$$P^{AB}_{\alpha\beta,\tau} = -i(P^{AB,I}_{\alpha\beta,\tau} + P^{AB,II}_{\alpha\beta,\tau} + P^{AB,III}_{\alpha\beta,\tau} + P^{AB,IV}_{\alpha\beta,\tau}) \tag{41}$$

where

$$\begin{aligned} P^{AB,I}_{\alpha\beta,\tau} &= \sum_{\mu\nu\kappa\lambda} C^{DAA}_{\lambda\mu\alpha} \underline{G}^{DC}_{\lambda\kappa,\tau} \bar{G}^{AB}_{\mu\nu,\tau} C^{CBB}_{\kappa\nu\beta} \\ P^{AB,II}_{\alpha\beta,\tau} &= \sum_{\mu\nu\kappa\lambda} C^{DAA}_{\lambda\mu\alpha} \underline{G}^{AC}_{\mu\kappa,\tau} \bar{G}^{DB}_{\lambda\nu,\tau} C^{CBB}_{\kappa\nu\beta} \\ P^{AB,IV}_{\alpha\beta,\tau} &= \sum_{\mu\nu\kappa\lambda} C^{DAA}_{\lambda\mu\alpha} \underline{G}^{AB}_{\mu\nu,\tau} \bar{G}^{DC}_{\lambda\kappa,\tau} C^{CBB}_{\kappa\nu\beta} \end{aligned} \tag{42}$$

As $\underline{G}$ and $\bar{G}$ are symmetric, the symmetry of the Kronecker product implies that P is symmetric as well and consequently $P^{AB,III} = [P^{BA,II}]^T$ and $P^{AB} = [P^{BA}]^T$. Also note that $Re(P) = 0$. With the definition of the intermediates

$$\underline{F}^{ABB}_{\mu\nu\beta,\tau} = \sum_{\kappa} \underline{G}^{AC}_{\mu\kappa,\tau} C^{CBB}_{\kappa\nu\beta} \tag{43}$$

$$\bar{F}^{ABB}_{\mu\nu\beta,\tau} = \sum_{\kappa} \bar{G}^{AC}_{\mu\kappa,\tau} C^{CBB}_{\nu'\nu\beta} \tag{44}$$

$$\underline{H}^{ACB}_{\mu\kappa\beta,\tau} = \sum_{\nu} \underline{F}^{ABB}_{\mu\nu\beta,\tau} \bar{G}^{BC}_{\nu\kappa,\tau} \tag{45}$$

$$\bar{H}^{ACB}_{\mu\kappa\beta,\tau} = \sum_{\nu} \bar{F}^{ABB}_{\mu\nu\beta,\tau} \underline{G}^{BC}_{\nu\kappa,\tau} \tag{46}$$

eq 42 is most conveniently evaluated as

$$\begin{aligned} P^{AB,I}_{\alpha\beta,\tau} + P^{AB,IV}_{\alpha\beta,\tau} &= \sum_{\nu\kappa} (\underline{H}^{CBA}_{\kappa\nu\alpha,\tau} + \bar{H}^{CBA}_{\kappa\nu\alpha,\tau}) C^{CBB}_{\kappa\nu\beta} \\ P^{AB,II}_{\alpha\beta,\tau} &= \sum_{\mu\nu} \bar{F}^{BAA}_{\nu\mu\alpha,\tau} \underline{F}^{ABB}_{\mu\nu\beta,\tau} \end{aligned} \tag{47}$$

We parallelize the outermost loop over all atoms and perform all tensor contractions using level-3 BLAS. No step involves more than three atomic centers, and since tensor contractions corresponding to distant centers (for which all elements in C are zero) can be skipped, the operation count scales asymptotically as N^2. We always evaluate the intermediate eqs 43−46 on the fly since the storage of 2-center quantities with more than 2 indices would quickly become prohibitive.

2.3.3. Screened Coulomb Interaction. Having evaluated P for all atom pairs, $\tilde{W}$ can be evaluated. After transforming the matrix P (which is even in imaginary time) to the imaginary frequency axis using (40), the screened interaction $\tilde{W}_\omega$ is obtained by inversion

$$\tilde{W}_\omega = [V^{-1} - P_\omega]^{-1} - V \tag{48}$$

For all ω, W is stored in distributed memory. Note that, on the imaginary frequency axis, $\mathrm{Im}(P) = 0$ and thus $\mathrm{Im}(\tilde{W}) = 0$ as well. To evaluate (48), the dielectric function is not constructed explicitly as it would not be symmetric and its inversion would be computationally demanding. We invert $V^{-1} - P_\omega$ (and V which only needs to be done once) using an LU decomposition with partial pivoting as implemented in SCALAPACK. Note that inversion using CD would be numerically unstable since C might not be full-rank and thus does not necessarily conserve positive semi-definiteness. We subsequently transform $\tilde{W}$ back to imaginary time.

2.3.4. Self-Energy. Next, the contributions to Σ for all atom pairs

$$\Sigma^{c,AB}_{\mu\nu,\tau} = i(\Sigma^{AB,I}_{\mu\nu,\tau} + \Sigma^{c,AB,II}_{\mu\nu,\tau} + \Sigma^{c,AB,III}_{\mu\nu,\tau} + \Sigma^{c,AB,IV}_{\mu\nu,\tau}) \tag{49}$$

are evaluated, where $\Sigma^{AB,III} = [\Sigma^{BA,II}]^T$ and $\Sigma^{AB} = [\Sigma^{BA}]^T$. Also, $Re(\Sigma^c) = 0$, since $Re(G) = 0$ and $Re(\tilde{W}) = 0$. We only give here the equations for $\Sigma^c(i\tau)$ as Σ^x is obtained in exactly the same way by replacing $\tilde{W}$ with V and using $\underline{G}(i\tau = 0)$. As Σ is an uneven function in imaginary time, we also need to evaluate $\Sigma(-i\tau)$ to be able to Fourier transform it to the imaginary frequency axis. The corresponding equations can be retrieved from the ones for $\Sigma(i\tau)$ by simply exchanging $\underline{G}$ with $\bar{G}$ and replacing upper bars with lower bars in all the intermediates. To express the individual contributions to Σ, we define the intermediate

$$I^{ABC}_{\mu\nu\gamma,\tau} = C^{ABB}_{\mu\nu\beta} \tilde{W}^{BC}_{\beta\gamma,\tau} \tag{50}$$

and together with (44) and (43) we obtain

$$\underline{\Sigma}^{c,AC,I}_{\mu\kappa,\tau} = \sum_{\nu\lambda} \sum_{\alpha\gamma} \underline{G}^{DB}_{\lambda\nu,\tau} C^{DAA}_{\lambda\mu\alpha} \tilde{W}^{AC}_{\alpha\gamma,\tau} C^{BCC}_{\nu\kappa\gamma} = \sum_{\nu\alpha} \underline{F}^{BAA}_{\nu\mu\alpha,\tau} I^{BCA}_{\nu\kappa\alpha,\tau} \tag{51}$$

$$\underline{\Sigma}^{c,AC,II}_{\mu\kappa,\tau} = \sum_{\nu\lambda} \sum_{\alpha\beta} \underline{G}^{DB}_{\lambda\nu,\tau} C^{DAA}_{\lambda\mu\alpha} \tilde{W}^{AB}_{\alpha\beta,\tau} C^{CBB}_{\kappa\nu\beta} = \sum_{\nu\alpha} \underline{F}^{BAA}_{\nu\mu\alpha,\tau} I^{CBA}_{\kappa\nu\alpha,\tau} \tag{52}$$

$$\begin{aligned} \underline{\Sigma}^{c,AC,IV}_{\mu\kappa,\tau} &= \sum_{\nu\lambda} \sum_{\delta\beta} \underline{G}^{DB}_{\lambda\nu,\tau} C^{ADD}_{\mu\lambda\delta} \tilde{W}^{DB}_{\delta\beta,\tau} C^{CBB}_{\kappa\nu\beta} \\ &= \sum_{\lambda\delta} \left[\sum_{\nu} \underline{G}^{DB}_{\lambda\nu,\tau} I^{CBD}_{\kappa\nu\delta,\tau} \right] C^{ADD}_{\mu\lambda\delta} \end{aligned} \tag{53}$$

As for P, we parallelize the outermost loop over all atoms and perform all tensor contractions using level-3 BLAS routines. Due to its prefactor of $N_{AO,l}{}^2 \times N_{\mathrm{aux},l}{}^2$, where $N_{\mathrm{aux},l}$ ($N_{AO,l}$) denotes the number of ABFs (AOs) on on atomic center, the calculation of I is the most expensive step. The asymptotic operation count can be reduced significantly since the screened interaction $\tilde{W}$ decays exponentially as a direct consequence of the exponential decay of the Green's function, unlike the bare Coulomb interaction. In our current implementation, we do not fully exploit this property as we essentially treat $\tilde{W}$ like the

https://dx.doi.org/10.1021/acs.jctc.0c00693
J. Chem. Theory Comput. 2020, 16, 7381−7399

bare Coulomb potential in the calculation of Σ^x. In the same way as for C, we can skip all tensor contractions for approximately non-Coulomb-interacting atom pairs. For weakly interacting pairs, we rely on multipole expansion of the Coulomb potential to reduce the prefactor of all contractions involving W (and V for Σ^x) considerably so that Σ can also be evaluated with a quadratic operation count only. When one fully exploits the exponential decay of $\tilde{W}$, the asymptotic scaling can possibly be reduced further.

2.3.5. Quasi-Particle Equations. Σ^c is subsequently transformed to the MO basis and its diagonal elements, to the imaginary frequency space. With (40),

$$\Sigma^c_{nn,\omega_k} = -i \sum_j \gamma^{(c)}_{kj} \cos(\omega_k \tau_j)[\Sigma^c_{nn,\tau_j} + \bar{\Sigma}^c_{nn,\tau_j}] - \sum_j \gamma^{(s)}_{kj} \sin(\omega_k \tau_j)[\Sigma^c_{nn,\tau_j} - \bar{\Sigma}^c_{nn,\tau_j}] \tag{54}$$

which we use to solve the QP equations (eq 10). We analytically continue (AC) Σ^c_{nn} to the real frequency axis using a Padé-approximant of order N_ω as described by Vidberg and Serene[208] and solve (10) for all states of interest using the bisection method. While the present approach is not applicable to core level excitations,[45−47] it predicts QP energies in the valence region with good accuracy in cases where the QP solution is sufficiently distant from any pole of the self-energy.[46,133,209,210] This is always the case for molecules with a large KS HOMO−LUMO gap. Note that in these cases small imaginary frequency grids are sufficient to ensure good accuracy for particle and hole states in the valence region.

To summarize this section, a pseudocode of our implementation together with the theoretical asymptotic scaling with the system size is given in Chart 1.

Chart 1

Algorithm 1 Pseudocode for G_0W_0 using PADF. The asymptotic operation count of some key steps is given on the right.

```
Input MO coefficients b_μn, orbital energies, ϵ_n from (1)
Compute C, V, V^-1
Compute {τ_i}_{i=1,...,N_τ}, {ω_k}_{k=1,...,N_ω}, {γ^(c)_ki, γ^(s)_ki}_{k=1,...,N_ω, i=1,...,N_τ}

for τ = τ_1, τ_2, τ_3 ..., τ_{N_τ} do
    Calculate G using (15), (16)                                   N^3 N_τ
    for A ∈ N_atom, B ∈ N_atom do
        Evaluate P^AB(τ_i) using (41)-(47)                         N^2 N_τ
    end for
    for ω = ω_1, ω_2, ω_3 ..., ω_{N_ω} do
        Calculate contribution to P(ω_i) using (40)                N^2 N_τ N_ω
    end for
end for
for ω = ω_1, ω_2, ω_3 ..., ω_{N_ω} do
    Calculate W(ω_k) using (48)                                    N^3 N_ω
end for
for τ = τ_1, τ_2, τ_3 ..., τ_{N_τ} do
    for ω = ω_1, ω_2, ω_3 ..., ω_{N_ω} do
        Calculate W(τ_i) using (40)                                N^2 N_τ N_ω
    end for
    for A ∈ N_atom, B ∈ N_atom do
        Evaluate Σ^AB(τ_i) using (49) to (53)                      N^2 N_τ
    end for
    Calculate Σ_{nn,τ_i} and evaluate (54)
end for
Evaluate QP-spectrum using (10)
```

3. RESULTS

3.1. Computational Details. All calculations have been performed with a locally modified development version of ADF[172,173] in which the herein described PADF-G_0W_0 algorithm has been implemented. In all gKS calculations, PADF has been used to evaluate Coulomb and exchange terms.[149,150,211] We performed PADF-G_0W_0@PBE and PADF-G_0W_0@PBE0 calculations for all molecules in the GW100 database[82] as well as PADF-G_0W_0@PBE0[212,213] calculations for selected molecules from the GW5000 database.[214] For GW100, we used the structures as published in the original work,[82] except for vinyl bromide and phenol for which we used the updated structures.[215] To preclude potential confusion, we emphasize that all results from the other codes we refer to herein have been taken from the literature and have not been calculated by us.

We herein use several all-electron (AE) STO-type basis sets of double-ζ (DZ), TZ, and QZ size. The prefix "aug-" denotes augmentation of a basis set with an additional shell of diffuse functions for all angular momenta l = 0, 1, and 2. For augmented QZ basis sets, an additional diffuse shell of f-functions is added as well. Augmentation of the basis set with x additional shells of polarization functions is denoted by xP. We employ two different QZ basis sets: the even-tempered QZ3P[216] basis set and the larger QZ4P[217] basis set. For a detailed description of the basis sets, see van Lenthe and Baerends.[217] It should be noted, however, that all basis sets are not correlation consistent (CC) and unsuitable for CBS limit extrapolation. Also note that QZ3P and all augmented basis sets are only available for the first 4 rows of the periodic table. In the case of QZ3P, we will use QZ4P for all heavier elements, and in the case of the augmented basis sets, we use the respective basis set without augmentation.

If not indicated otherwise, we used the *Normal* auxiliary fit set,[218] *Good* quality for numerical integration,[211] *Normal* quality for thresholds controlling distance effects, and standard numerical settings otherwise. We use imaginary time and frequency grids with up to $N_\omega = N_\tau = 18$ points each[219] for GW100 and $N_\omega = N_\tau = 16$ points each for GW5000 and use a padé-approximant of order N_ω to model the self-energy on the real frequency axis. In all G_0W_0@*PBE*0 calculations on GW5000, we used the unscaled Zero Order Regular Approximation (ZORA).[220−223]

During orthonormalization of the Fock matrix in the SCF, we remove columns of the transformation matrix when the corresponding eigenvalues of the AO-overlap matrix are smaller than some threshold ϵ_D.[196] As explained above, we have adjusted this value to $\epsilon_D = 10^{-3}$ in all calculations using QZ4P or augmented basis sets. Otherwise, the default of $\epsilon_D = 10^{-4}$ has been used.

3.2. Benchmarks. *3.2.1. The GW100 Database.* The size and type of the single-particle basis are the most crucial factors influencing the results of a GW calculation.[82] Using localized basis functions, even on the QZ level, BSEs for HOMO and especially LUMO QP energies can exceed several hundred meV, necessitating a CBS limit extrapolation to obtain very accurate reference values.[46,82,214] Using localized AOs, one needs to rely on heuristics since the expansion of MOs in this basis does not converge uniformly, unlike expansions in terms of PW[224] or finite elements in RS.[225] HOMO QP energies obtained with these basis set types are generally in good agreement with the original ones by van Setten et al.,[82] while differences for unbound LUMO energies often exceed 1 eV.[210,226,227]

Thus, it is not straightforward for our purpose to chose appropriate reference values, and we will therefore use more than one reference in the following. As a primary reference for GW100, we use RS results[228] by Gao and Chelikowsky.[227] While these results are not extrapolated to the CBS limit, they

https://dx.doi.org/10.1021/acs.jctc.0c00693
J. Chem. Theory Comput. 2020, 16, 7381−7399

are carefully converged and should be a very reliable reference. This choice is mainly motivated by the large differences between plane-wave and GTO implementations for unbound LUMO energies. It has been argued by Kresse and co-workers[226] that the GTO-type basis sets of the def2 family might not be flexible enough to adequately describe these QP energies and lead to significantly overestimated unbound LUMO energies. As also pointed out in ref 226, CC GTO-type basis sets are much more suitable in this respect; however, since we are not aware of reference values for GW100, this is not an option for benchmarking. On the other hand, the nanoGW results deviate to WEST/VASP by only 134/122 meV for GW100, only excluding all noble gases and H_2 but including all other molecules with unbound LUMOs.[227] While in comparisons between different codes these systems are often excluded,[210] we decided to retain them in this work. However, we excluded from our analysis all noble gases and H_2 since for these molecules the discrepancies between RS, PW-pseudopotential, and AE codes often exceed 2 eV.[82,210,226,227] We also excluded CI_4, KBr, NaCl, BN, O_3, BeO, MgO, Cu_2, and CuCN for which there are multiple solutions for the HOMO when the QP equation (10) is solved. This leaves us with a set of 85 molecules that we will discuss in the following. In Section 3.2.2, we benchmark our implementation against reference results obtained with GTOs for a large number of organic molecules with bound LUMOs.

The histograms in Figure 1 summarize the results of our benchmarks on GW100 and show errors obtained with our

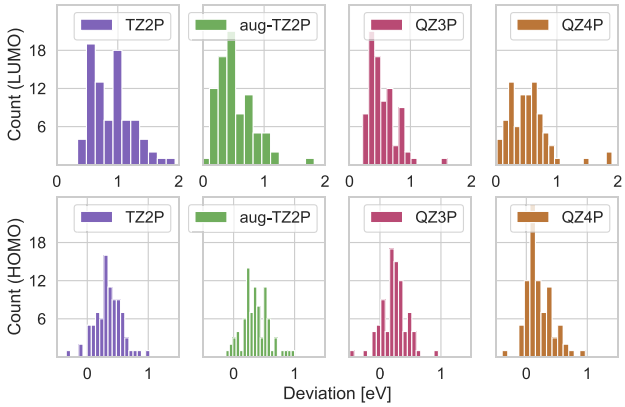

Figure 1. Error distributions (in eV) for G_0W_0@PBE with four different STO-type basis sets for the HOMO (bottom) and LUMO QP energies (top) in the GW100 database with respect to the nanoGW reference. Due to its error larger than 3 eV, CO_2 is not included in the upper left plot.

implementation and different basis sets with respect to the nanoGW reference. For individual QP energies, we refer to the Supporting Information. Figure 2 shows mean absolute deviations (MAD) for the HOMO QP energies between different codes and basis sets. Since we are not able to perform basis set extrapolation, the QZ4P results are the best ones attainable for us. We observe MADs of 0.24 eV with respect to the nanoGW[229] results and of 0.32 eV to the CBS limit extrapolated (CBSLE) FHI-AIMS[68,69,134] QP energies. With respect to both, the RS and the FHI-AIMS CBS limit, QZ4P yields an accuracy comparable to TURBOMOLE[230] with the smaller def2-TZVP basis set (sixth and seventh column in the heatmap in Figure 2). QZ4P does not give significant

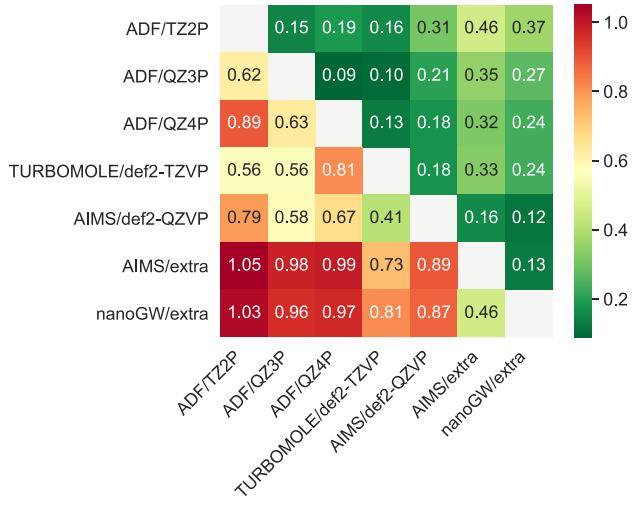

Figure 2. MADs (upper triangle) and maximum absolute deviations (lower triangle) in eV of QP HOMO energies computed with different codes and basis sets, specified on the axes for G_0W_0@PBE.[215]

improvements over QZ3P, and with a MAD of 0.12 eV with respect to the nanoGW reference, def2-QZVP performs considerably better than QZ4P. The fact that the former one has more polarization functions (e.g., (7s, 4p, 3d, 2f, 1g) vs (7s, 4p, 2d, 2f) for second row elements[231]) might explain part of the discrepancy. Furthermore, the excessive truncation of the QZ4P basis in the canonical orthonormalization procedure during the SCF effectively diminishes the size of the virtual space. This might also explain why QZ4P only improves moderately over the significantly smaller TZ2P basis set (0.46 vs 0.32 eV) while going from def2-TZVP to def2-QZVP reduces the MAD with respect to both CBS limits by roughly 50%. Also, a visual inspection of the error distributions for the QZ3P and QZ4P QP HOMO energies in Figure 1 reveals that the QZ4P errors show a larger spread and more often exceed 0.5 eV than those for QZ3P.

For the LUMO QP energies shown in the upper part of Figure 1, aug-TZ2P, QZ3P, and QZ4P show comparable MADs of 0.55, 0.56, and 0.52 eV, respectively, and thus improve significantly over TZ2P with a MAD of nearly 1 eV (see Table 1). For TZ2P and both QZ basis sets, the MAD of

Table 1. MADs of the G_0W_0@PBE HOMO and LUMO QP Energies Corresponding to Figure 1 and HOMO−LUMO Gaps with Respect to the CBS Limit for Four Different STO-Type Basis Sets[a]

	TZ2P	aug-TZ2P	QZ3P	QZ4P
HOMO	0.37	0.37	0.27	0.24
LUMO	0.94	0.55	0.56	0.52
gap	0.59	0.26	0.34	0.35

[a]All values in eV.

the LUMO QP energies with respect to the RS reference values is more than twice as large than for the HOMO, which results in a rather poor description of the HOMO−LUMO gap. This behavior is similar to the performance of the def2 family of GTO-type basis sets for GW100 for which the errors for the LUMO are on average roughly twice as large than for the HOMO.[82] aug-TZ2P overestimates HOMO and LUMO

https://dx.doi.org/10.1021/acs.jctc.0c00693
J. Chem. Theory Comput. 2020, 16, 7381−7399

QP energies most symmetrically and consequently, with a MAD of 0.26 eV, describes the HOMO−LUMO gap significantly better than both QZ basis sets. The situation is well-known from augmented GTO-type basis sets,[73,209,232−235] which usually converge considerably faster to the CBS HOMO−LUMO gap than the nonaugmented basis sets,[209] although the individual HOMO and LUMO levels are often not converged at all.

Finally, we investigate some LUMO QP energies with exceptionally slow convergence to the CBS limit in more detail and see whether convergence can be attained using larger basis sets, keeping in mind the restrictions imposed by the PADF as explained in Section 2; reaching the basis set limit is only possibly for us for very small systems. While the CO_2 LUMO QP energy deviates from the CBS limit by more than 3 eV, also for F_2, CF_4 C_3H_3, and C_nH_{2n+2} for n = 1, ..., 4, the TZ2P LUMO QP energies deviate between 1.7 and 1.4 eV from the CBS limit. We investigate the convergence with respect to the basis set size for these molecules (except for propane and butane) in Figure 3 by adding diffuse functions to the QZ3P basis set.

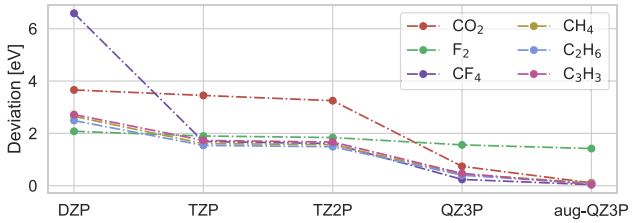

Figure 3. Deviations of G_0W_0@PBE LUMO QP energies to the CBS limit for six selected molecules from the GW100 database for different STO-type basis sets (all values in eV).

For all molecules except F_2, our aug-QZ3P results agree very well with the RS reference values. This is a little surprising since the GTO-type basis set CBSLE results differ by more than 1 eV for CH_4, C_2H_6, and C_3H_3. In fact, we observe not only for these systems that our unbound LUMO energies are generally closer to RS and PW than to GTO references. While being out of the scope of this work, this is an interesting observation that deserves further investigation. For F_2, the extrapolated CBS limits from different codes are in good agreement and the errors from aug-QZ3P are still hard to explain with BSEs alone, although van Setten et al. found a BSE of 0.53 eV for the LUMO energy using def2-QZVP.[82]

3.2.2. The GW5000 Database. We now turn our attention to systems large enough for local approximations to take effect and discuss the HOMO and LUMO energies of 20 organic molecules with in between 85 and 99 atoms from the GW5000 database.[214] These tests are crucial for our purpose. First, they allow us to assess the effect of the values of the thresholds controlling distance effects. As explained in detail elsewhere,[162] we essentially rely on three thresholds in our implementation, which we organize in three tiers, denoted as *Basic*, *Normal*, and *Good*. For the exact values of these thresholds, we refer to the Supporting Information.

The convergence with respect to the threshold tiers for HOMO and LUMO QP energies is shown in Figure 4. As shown in the lower panel, the HOMO energies from different threshold tiers agree within 0.1 eV, and the HOMO energies from the *Normal* and the *Good* threshold tier usually agree

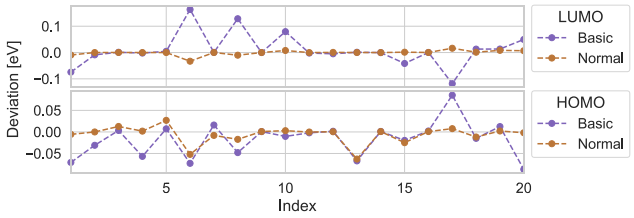

Figure 4. Deviations of the *Basic* and *Normal* threshold tiers with respect to the *Good* tier for HOMO (bottom) and LUMO (top) QP energies on the G_0W_0/PBE0 level of theory (all values are in eV).

within an accuracy of 60 mEV. Using the *Basic* threshold tier, the LUMO QP energies show a maximum deviation of roughly 0.15 meV with respect to the *Good* tier. On the other hand, the LUMO energies from the *Normal* and *Good* tier are in even better agreement than the corresponding HOMO energies. Thus, using the *Normal* tier ensures an internal precision of our implementation of 60 meV for HOMO and LUMO QP energies. In case only the HOMO level is of interest, sufficient precision is already attained using the *Basic* threshold tier.

Second, the applicability of our implementation to the small molecules in GW100 does not automatically imply the same for larger systems. In fact, this is true for any method exploiting locality in any form. Due to the reasons outlined in Section 2, we refrain from reporting results with QZ and large augmented basis sets for these systems. Instead, we want to investigate the accuracy attainable using the TZ2P and aug-DZP basis sets for which no numerical problems can be expected also for large molecules.

We compare our results for QP HOMO and LUMO levels as well as the HOMO−LUMO gap for the 20 selected molecules to accurate reference values calculated with numerical GTOs with the FHI-AIMS code in Figure 5.

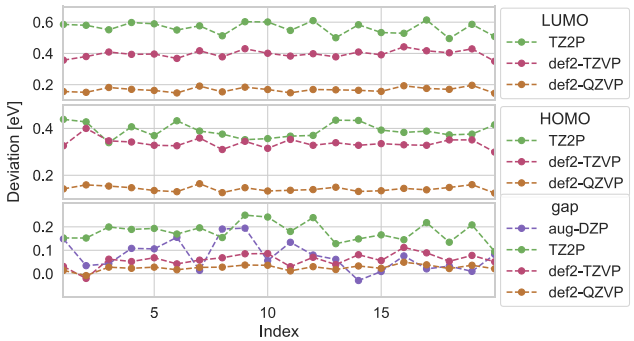

Figure 5. Deviations of LUMO (upper panel) QP energies, HOMO (middle panel) QP energies, and HOMO−LUMO QP gaps (lower panel) for the TZ2P (*Normal* thresholds) as well as the GTO-type def2-TZVP and def2-QZVP basis sets with respect to the CBS limit for the HOMO energies of the 20 large molecules from the GW5000 database. HOMO−LUMO QP gaps from aug-DZP are shown as well. All values are in eV.

MADs for these quantities with respect to the CBS limit are given in Table 2. We observe that the TZ2P HOMO QP energy never deviates from def2-TZVP by more than 0.1 eV and the MAD of 0.39 eV is only 50 meV higher than the one found for def2-TZVP. For the LUMO energy, the situation is different. While def2-TZVP yields a MAD of 0.40 eV for this quantity, TZ2P performs considerably worse with 0.56 eV.

https://dx.doi.org/10.1021/acs.jctc.0c00693
J. Chem. Theory Comput. 2020, 16, 7381−7399

Table 2. MADs of HOMO Energies, LUMO Energies, and HOMO−LUMO Gaps with Respect to the CBS Limit for the 20 Considered Molecules from the GW5000 Database for Different Basis Sets[a]

	def2-TZVP	def2-QZVP	TZ2P	aug-DZP
HOMO	0.34	0.14	0.39	0.46
LUMO	0.40	0.17	0.56	0.53
gap	0.06	0.03	0.18	0.08

[a]The *Normal* tier of the thresholds has been used in all PADF-G_0W_0 calculations. All values are in eV.

This has a profound effect on the description of the HOMO−LUMO gap. Since def2-TZVP overestimates the LUMO level not much more than the HOMO QP energy, the HOMO−LUMO gap shows a MAD of 0.06 eV, which is in excellent agreement to the CBS limit, while TZ2P yields a MAD of 0.17 eV. On the other hand, using the smaller aug-DZP basis set, we find a MAD of 0.08 eV, in good agreement with the CBS limit. As might be inferred from Table 2, this success results mainly in a poorer description of the HOMO level compared to TZ2P, and the error cancellation between HOMO and LUMO is not always reliable, which can be seen from systems #8 and #9 whose HOMO−LUMO gap differs from the CBS limit by 0.2 eV. It should also be noted that aug-DZP calculations are slightly slower than TZ2P ones for medium and large systems since more AO-pair products need to be considered.

Finally, we investigate the accuracy of our algorithm as a function of the system size. To this end, we randomly selected 250 molecules from the GW5000 database and sorted these systems from smallest (12 atoms) to largest (99 atoms). Figure 6 shows the deviations from the CBS limit of our G_0W_0@PBE0

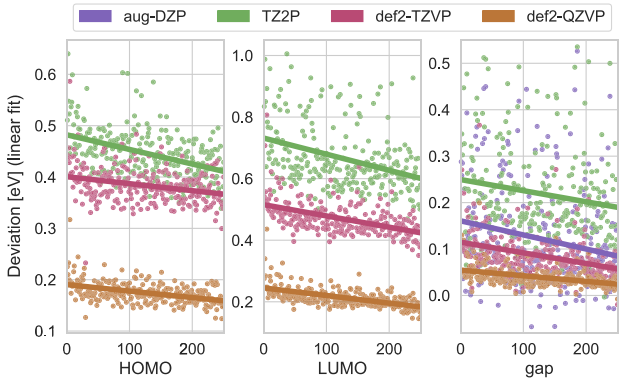

Figure 6. Errors with respect to the CBS limit for HOMO (left) and LUMO QP energies (middle) as well as HOMO−LUMO QP gaps (right) with different basis sets for 250 randomly selected molecules from the GW5000 database (dots) as well as linear fits, $f(x) = a \times x + b$. The systems have been sorted according to increasing size.

results for the HOMO, LUMO, and HOMO−LUMO QP gap with the TZ2P and aug-DZP basis sets as well as FHI-AIMS results using the def2-TZVP and def2-QZVP basis sets.[214] Additionally, we performed linear fits as implemented in Numpy,[236] which are also shown in Figure 6. Essentially, we obtain the same picture as for the 20 large molecules: TZ2P performs nearly as good as def2-TZVP for the HOMO QP energies and considerably worse for the LUMO level, which translates into a worse description of the HOMO−LUMO gap. While it is observed that the STO results show a larger spread than their GTO counterparts especially for LUMO energies, we also observe that the deviation from the CBS limit decreases with increasing system size for all basis sets. For all subplots in Figure 6, the TZ2P fit is more or less parallel (also see the fit parameters in the Supporting Information for comparison) to the GTO fits, while the slope in the aug-DZP fit for the HOMO−LUMO gap is slightly more negative. In the same way as for the subset of 20 large molecules, aug-DZP produces HOMO−LUMO gaps that on average agree with the CBSLE reference within 0.15 eV for systems larger than a few tens of atoms. However, in some cases the errors can still be rather large (e.g., larger than 0.4 eV in 7 out of 250 cases), while the def2-QZVP BSE practically never exceeds 0.1 eV.

The decreasing errors are most likely due to basis set superposition, which leads to a more complete basis when the system increases, and the assumption that this effect is more pronounced for basis sets with many diffuse functions such as aug-DZP is reasonable. Thus, we can conclude that the accuracy of our algorithm is not negatively affected when the system size is increased . We note that local overcompleteness and the associated numerical issues can already be encountered for very small systems like the ones on the left side of the plots in Figure 6. On the other hand, it is highly unlikely that they become more pronounced for larger systems due to the locality of the AOs.

3.3. Representative Timings. In order to analyze the asymptotic scaling of our algorithm, we present G_0W_0@PBE/TZ2P calculations on a series of water clusters[237] using the same numerical settings as for GW5000, the *Basic* and *Normal* tiers of thresholds, and 12 imaginary time and imaginary frequency points. All calculations presented in this subsection were performed on 2.2 GHz intel Xeon (E5-2650 v4) nodes (broadwell architecture) with 24 cores and 128 GB RAM each (bw nodes in short). Figure 7 shows the wall times for the

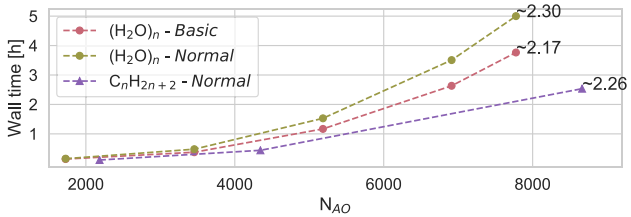

Figure 7. Wall times in hours for G_0W_0@PBE/TZ2P calculations on a series of water clusters and a linear alkane chain (excluding the preceding SCF). All calculations have been performed on 2 bw nodes. The exponent of the polynomial describing the asymptotic scaling of the algorithm is given on the right of each plot.

G_0W_0 part of the calculations and the exponents of the polynomials describing the asymptotic scaling of these calculations with increasing system size. The information on CPU time and asymptotic scaling of the key steps of the algorithm for the largest of these systems are given in Figure 8.

The largest water cluster here comprises 432 atoms with 7776 AOs and 36 576 ABFs. Using the *Normal* threshold tier, the whole G_0W_0 calculation takes 5 h on two nodes. As shown in Figure 8, the most expensive step is the calculation of Σ, which is responsible for about half of the wall time of the whole calculation, followed by the evaluation of P. The evaluation of Σ is also the step that is accelerated most when the thresholds are loosened. This is due to the contractions (eq

https://dx.doi.org/10.1021/acs.jctc.0c00693
J. Chem. Theory Comput. 2020, 16, 7381−7399

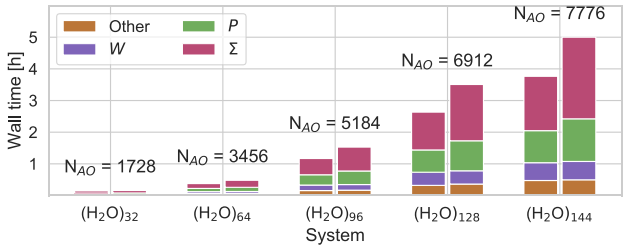

Figure 8. Contributions to total G_0W_0 wall times from different key steps for a series of water clusters using the TZ2P basis set. Left bar in each group: *Basic* threshold quality; right bar in each group: *Normal* threshold quality. All calculations have been performed on 2 bw nodes.

50), which are tremendously accelerated when the multipole approximation is used for an increasing number of atom pairs. Consequently, the asymptotic scaling of this step is decreased from $N^{2.34}$ to $N^{2.15}$. Also, the asymptotic scaling of P is reduced considerably (from $N^{2.19}$ to $N^{2.05}$), so that the wall time of the total calculation can be reduced to less than 4 h. Note that the evaluation of W is not affected by changing the thresholds and asymptotically scales as N^3. However, even for the largest water cluster considered here, the timings are clearly dominated by P and Σ and the calculation of W can not be expected to become a bottleneck even for much larger systems.

Water clusters are very compact systems due to their spherical shapes. For low-dimensional systems, the asymptotic scaling is actually worse (since N^3 steps become more important) while the overall calculations are considerably faster. The timings for a series of linear alkane chains is given for comparison in Figure 7. With the same thresholds, the G_0W_0 calculation for $C_{160}H_{322}$ takes roughly 2.5 h, only half the time as the one for $(H_2O)_{144}$ even though the former system is larger. In fact, P is calculated in less than half an hour, which is less wall time than is required for the calculation of $\tilde{W}$.

Next, we investigate scaling with respect to the single-particle basis at a fixed system size. As shown in Figure 9, even

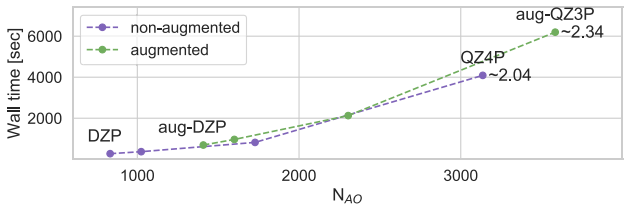

Figure 9. Timings (in seconds) and the asymptotic scaling of our algorithm with basis sets of increasing size for $(H_2O)_{32}$ with the same settings as described above (*Normal* thresholds) using a single bw node.

for the small $(H_2O)_{32}$ cluster, our algorithm scales quadratically with the size of the single-particle basis when non-augmented basis sets are used. Using augmented basis sets, the asymptotic scaling is worse owing to the large number of basis functions with a very slow decay with the distance to the nuclei on which they are centered, leading to a smaller number of negligible AO products. High scaling with respect to the single-particle basis is a general shortcoming of AO-based algorithms compared to MO-based ones, and it is difficult to envisage how our algorithm might be modified to overcome this issue.

Finally, we comment on the parallel performance of our algorithm. Figure 10 shows the speedup with increasing

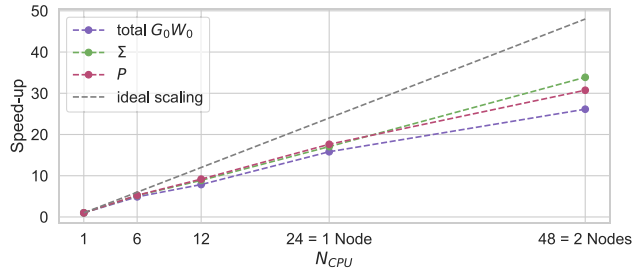

Figure 10. Speedup for $(H_2O)_{64}$ (the same settings as described above, *Normal* thresholds) with the number of CPUs.

number of cores. We achieve a parallel efficiency of 66% when going from 1 to 24 cores. The deviation from the ideal speedup is partly due to small fractions of the serial code in our algorithm but also due to unnecessary network communication. Also due to the latter factor, the parallelization over multiple nodes is less efficient. At the moment, our algorithms for the calculation of P and Σ communicate a lot of data, an aspect that we have not optimized yet.

For completeness, we also mention the large memory count of our algorithm increasing as N^2 with the system size. However, the practical memory bottleneck is rather the storage of C. Although only linearly scaling, we store it in shared memory, which prevents the scalability of our algorithm to even larger systems. The memory requirements are reduced for low-dimensional systems for which C becomes smaller; however, it is clear that the systems much larger than the ones presented herein can not be treated any more. Still, for systems of hundreds of atoms for which conventional implementations require a supercomputer,[98,99] G_0W_0 calculations with our algorithm can be performed in a routine fashion, which puts its application in mainstream computational spectroscopy within reach.

4. CONCLUSION

In this work, we have presented a PADF-based G_0W_0 implementation using STOs and relying on an imaginary time representation of the single-particle Green's function. Our algorithm combines quadratic scaling in memory and operation count with a very small prefactor due to a sparse map from the ABF space to the AO product space. Using realistic numerical settings, a G_0W_0 calculation for a spherically shaped water cluster with 432 atoms, 7776 AOs, and 36 576 ABFs takes 240 CPU hours. Using slightly looser thresholds, the same calculation is done in 180 CPU hours and the G_0W_0 calculations for a linear alkane chain with the same number of AOs takes only about 100 CPU hours. Thus, our algorithm is at least 1 order of magnitude faster than the fastest state-of-the-art canonical implementations.[99,209]

The accuracy of our algorithm for the calculation of the HOMO and LUMO QP energies in the GW100 database has been investigated by comparison to accurate RS reference values. We found MADs of 0.37 eV for TZ2P and 0.24 eV for QZ4P for the HOMO and 0.94 eV for TZ2P and 0.52 eV for QZ4P for the LUMO energies, respectively. For the HOMO level, FHI-AIMS/def2-QZVP only deviates from the CBS limit by 0.12 eV on average and TURBOMOLE/TZVP deviates by

https://dx.doi.org/10.1021/acs.jctc.0c00693
J. Chem. Theory Comput. 2020, 16, 7381−7399

0.24 eV. Thus, for GW100, our algorithm is only slightly more accurate on the QZ4P level as canonical implementations using def2-TZVP (where one should keep in mind that QZ4P is smaller than def2-QZVP) while it is difficult to make a definite statement about the quality of our LUMO energies due to large discrepancies between different codes.[82,210,226,227]

Larger basis set errors aside, two factors are responsible for the relatively poor performance of our algorithm for GW100. First, for many systems with QP solutions close to the poles of the self-energy, our frequency treatment with AC is inaccurate and we often observe large differences with respect to the reference. This feature is also observed within other closely related schemes.[99,226] As expected,[210] this issue is mostly avoided when a gKS reference is used. Certainly, using a more sophisticated algorithm to generate larger imaginary frequency grids than the present ones, which are limited to a maximum of 19 points, will also improve our algorithm for systems with a small KS HOMO−LUMO gap and/or low-lying core states for which generally higher resolution on the frequency axes is required.[238]

Second, to also retain numerical stability of the PADF approach for large basis sets, parts of the unoccupied space need to be projected out during the SCF, which effectively diminishes the size of the basis set, especially when the basis set comprises many diffuse functions. This shortcoming can be traced back to the intrinsic difficulty of representing highly delocalized AO-pair densities using ABFs centered on two atoms only. With our auxiliary fit sets having been optimized for gKS calculations, this can lead to very large fitting coefficients, which in turn cause numerical instabilities. This issue is of a technical nature and can possibly be resolved by adding more diffuse functions with high angular momenta to our current auxiliary basis sets.[160] Employing auxiliary basis sets optimized for correlated methods, as it is common practice in global DF,[239−245] seems to be a promising route to approach the accuracy of canonical G_0W_0 also for large QZ basis sets and large systems.

Using smaller basis sets of augmented DZ and TZ quality, we calculated the HOMO and LUMO energies of a set of 250 organic molecules between 12 and 99 atoms from the GW5000 database and observed that the deviation from the FHI-AIMS CBSLE reference, not only within our scheme but also within the canonical scheme using the GTO-type basis sets, is actually decreasing with an increasing system size. Thus, we conclude that PADF-G_0W_0 calculations on the augmented DZ and TZ level can safely be performed for large systems as well. For another subset of GW5000 comprising 20 large molecules with in between 85 and 99 atoms, the aug-DZP HOMO−LUMO gap deviates by only 0.08 eV on average from the CBS limit, which is comparable to the FHI-AIMS/def2-TZVP reference.

To summarize, it is clear that further technical improvements of our algorithm are needed. Nevertheless, the examples in this work demonstrate that already in its current form it enables accurate G_0W_0 calculations for large systems of hundreds of atoms with TZ and augmented DZ basis sets in a routine fashion. Not only its scalability, but also its very small prefactor make it amenable to quasi-particle and fully self-consistent GW calculations, which are possible with straightforward extensions of our algorithm since we construct the complete Σ instead of only its diagonal in the MO basis. Due to the usually consistent overestimation of QP energies, BSEs often compensate each other to a large extent in calculations of HOMO−LUMO gaps, and in the past, many GW calculations with augmented DZ basis sets have provided important insights into the electronic properties of practically relevant systems.[73,209,232−235] This indicates that our algorithm might prove to be useful in practice already in its current form, e.g., in the study of large organic chromophores in solution or donor−acceptor systems, and we think that its computational efficiency outweighs its current limitations to reach the CBS limit with guaranteed accuracy.

■ ASSOCIATED CONTENT

Supporting Information

The Supporting Information is available free of charge at https://pubs.acs.org/doi/10.1021/acs.jctc.0c00693.

All calculated QP HOMO and LUMO energies for the GW100 and the subsets of the GW5000 database and fit parameters for Figure 6 and additional plots; explicit values for thresholds controlling distance effects as well as some explanations (PDF)

Imaginary frequency grids for some orbital energy ranges serving as starting values for our Levenberg−Marquardt algorithm as well as the corresponding errors of the approximate quadratures of the MP2 energy denominator (ZIP)

■ AUTHOR INFORMATION

Corresponding Author

Arno Förster − *Theoretical Chemistry, Vrije Universiteit, NL-1081 HV Amsterdam, The Netherlands;* orcid.org/0000-0002-0957-4081; Email: a.t.l.foerster@vu.nl

Author

Lucas Visscher − *Theoretical Chemistry, Vrije Universiteit, NL-1081 HV Amsterdam, The Netherlands;* orcid.org/0000-0002-7748-6243

Complete contact information is available at: https://pubs.acs.org/10.1021/acs.jctc.0c00693

Notes

The authors declare no competing financial interest.

■ ACKNOWLEDGMENTS

This research received funding from The Netherlands Organisation for Scientific Research (NWO) in the framework of the Innovation Fund for Chemistry and from the Ministry of Economic Affairs in the framework of the "*TKI/PPS-Toeslagregeling*".

■ REFERENCES

(1) Jensen, P.; Bunker, P. R. *Computational molecular spectroscopy*; Wiley, 2000.

(2) Parson, W. W. *Modern Optical Spectroscopy*; Springer: Berlin Heidelberg, 2007.

(3) Martin-Drumel, M. A.; McCarthy, M. C.; Patterson, D.; McGuire, B. A.; Crabtree, K. N. Automated microwave double resonance spectroscopy: A tool to identify and characterize chemical compounds. *J. Chem. Phys.* **2016**, *144*, 124202.

(4) Sugiki, T.; Kobayashi, N.; Fujiwara, T. Modern Technologies of Solution Nuclear Magnetic Resonance Spectroscopy for Three-dimensional Structure Determination of Proteins Open Avenues for Life Scientists. *Comput. Struct. Biotechnol. J.* **2017**, *15*, 328−339.

(5) Puzzarini, C.; Barone, V. Diving for Accurate Structures in the Ocean of Molecular Systems with the Help of Spectroscopy and Quantum Chemistry. *Acc. Chem. Res.* **2018**, *51*, 548−556.

(6) Choi, J. H.; Lee, H.; Lee, K. K.; Hahn, S.; Cho, M. Computational spectroscopy of ubiquitin: Comparison between theory and experiments. *J. Chem. Phys.* **2007**, *126*, No. 045102.
(7) Boukhvalov, D. W.; Katsnelson, M. I. Modeling of graphite oxide. *J. Am. Chem. Soc.* **2008**, *130*, 10697−10701.
(8) Zhang, W.; Carravetta, V.; Li, Z.; Luo, Y.; Yang, J. Oxidation states of graphene: Insights from computational spectroscopy. *J. Chem. Phys.* **2009**, *131*, 244505.
(9) Pedone, A.; Biczysko, M.; Barone, V. Environmental effects in computational spectroscopy: Accuracy and interpretation. *ChemPhysChem* **2010**, *11*, 1812−1832.
(10) Puzzarini, C.; Stanton, J. F.; Gauss, J. Quantum-chemical calculation of spectroscopic parameters for rotational spectroscopy. *Int. Rev. Phys. Chem.* **2010**, *29*, 273−367.
(11) Barone, V. *Computational strategies for spectroscopy: from small molecules to nano systems*; John Wiley & Sons, 2011.
(12) Berova, N.; Polavarapu, P. L.; Nakanishi, K.; Woody, R. W. *Comprehensive Chiroptical Spectroscopy: Instrumentation, Methodologies, and Theoretical Simulations*, 1st ed.; John Wiley & Sons, 2011.
(13) Barone, V.; Baiardi, A.; Biczysko, M.; Bloino, J.; Cappelli, C.; Lipparini, F. Implementation and validation of a multi-purpose virtual spectrometer for large systems in complex environments. *Phys. Chem. Chem. Phys.* **2012**, *14*, 12404−12422.
(14) Kessler, J.; Andrushchenko, V.; Kapitán, J.; Bouř, P. Insight into vibrational circular dichroism of proteins by density functional modeling. *Phys. Chem. Chem. Phys.* **2018**, *20*, 4926−4935.
(15) Puzzarini, C.; Bloino, J.; Tasinato, N.; Barone, V. Accuracy and Interpretability: The Devil and the Holy Grail. New Routes across Old Boundaries in Computational Spectroscopy. *Chem. Rev.* **2019**, *119*, 8131−8191.
(16) Kohn, W.; Sham, L. J. Self-Consistent Equations Including Exchange and Correlation Effects. *Phys. Rev.* **1965**, *140*, A1133.
(17) Hohenberg, P.; Kohn, W. Inhomogeneous Electron Gas. *Phys. Rev.* **1964**, *136*, B864−B871.
(18) Levy, M. Universal variational functionals of electron densities, first-order density matrices, and natural spin-orbitals and solution of the v-representability problem. *Proc. Natl. Acad. Sci. U. S. A.* **1979**, *76*, 6062−6065.
(19) Engel, E.; Dreizler, R. M. *Density Functional Theory: An Advanced Course*; Springer, 2013.
(20) Hickey, A. L.; Rowley, C. N. Benchmarking quantum chemical methods for the calculation of molecular dipole moments and polarizabilities. *J. Phys. Chem. A* **2014**, *118*, 3678−3687.
(21) Becke, A. D. Perspective: Fifty years of density-functional theory in chemical physics. *J. Chem. Phys.* **2014**, *140*, 18A301.
(22) Pribram-Jones, A.; Gross, D. A.; Burke, K. DFT: A Theory Full of Holes? *Annu. Rev. Phys. Chem.* **2015**, *66*, 283−304.
(23) Yu, H. S.; Li, S. L.; Truhlar, D. G. Perspective: Kohn-Sham density functional theory descending a staircase. *J. Chem. Phys.* **2016**, *145*, 130901.
(24) Goerigk, L.; Hansen, A.; Bauer, C.; Ehrlich, S.; Najibi, A.; Grimme, S. A look at the density functional theory zoo with the advanced GMTKN55 database for general main group thermochemistry, kinetics and noncovalent interactions. *Phys. Chem. Chem. Phys.* **2017**, *19*, 32184−32215.
(25) Mardirossian, N.; Head-Gordon, M. Thirty years of density functional theory in computational chemistry: An overview and extensive assessment of 200 density functionals. *Mol. Phys.* **2017**, *115*, 2315−2372.
(26) Grimme, S.; Schreiner, P. R. Computational Chemistry: The Fate of Current Methods and Future Challenges. *Angew. Chem., Int. Ed.* **2018**, *57*, 4170−4176.
(27) Godby, R. W.; Schlüter, M.; Sham, L. J. Self-energy operators and exchange-correlation potentials in semiconductors. *Phys. Rev. B: Condens. Matter Mater. Phys.* **1988**, *37*, 10159−10175.
(28) Engel, E.; Chevary, J. A.; Macdonald, L. D.; Vosko, S. H. Asymptotic properties of the exchange energy density and the exchange potential of finite systems: relevance for generalized gradient approximations. *Z. Phys. D: At., Mol. Clusters* **1992**, *23*, 7−14.
(29) Steinbeck, L.; Rubio, A.; Reining, L.; Torrent, M.; White, I. D.; Godby, R. W. Enhancements to the GW space-time method. *Comput. Phys. Commun.* **2000**, *125*, 105−118.
(30) Grüning, M.; Gritsenko, O. V.; Van Gisbergen, S. J.; Jan Baerends, E. On the required shape corrections to the local density and generalized gradient approximations to the Kohn-Sham potentials for molecular response calculations of (hyper)polarizabilities and excitation energies. *J. Chem. Phys.* **2002**, *116*, 9591−9601.
(31) Grüning, M.; Gritsenko, O. V.; Baerends, E. J. Exchange potential from the common energy denominator approximation for the Kohn-Sham Green's function: Application to (hyper)-polarizabilities of molecular chains. *J. Chem. Phys.* **2002**, *116*, 6435−6442.
(32) Malet, F.; Gori-Giorgi, P. Strong correlation in Kohn-Sham density functional theory. *Phys. Rev. Lett.* **2012**, *109*, 246402.
(33) Baerends, E. J.; Gritsenko, O. V.; Van Meer, R. The Kohn-Sham gap, the fundamental gap and the optical gap: The physical meaning of occupied and virtual Kohn-Sham orbital energies. *Phys. Chem. Chem. Phys.* **2013**, *15*, 16408−16425.
(34) Van Meer, R.; Gritsenko, O. V.; Baerends, E. J. Physical meaning of virtual kohn-sham orbitals and orbital energies: An ideal basis for the description of molecular excitations. *J. Chem. Theory Comput.* **2014**, *10*, 4432−4441.
(35) Gritsenko, O. V.; Mentel, M.; Baerends, E. J. On the errors of local density (LDA) and generalized gradient (GGA) approximations to the Kohn-Sham potential and orbital energies. *J. Chem. Phys.* **2016**, *144*, 204114.
(36) Baerends, E. J. From the Kohn-Sham band gap to the fundamental gap in solids. An integer electron approach. *Phys. Chem. Chem. Phys.* **2017**, *19*, 15639−15656.
(37) Thygesen, K. S.; Rubio, A. Nonequilibrium GW approach to quantum transport in nano-scale contacts. *J. Chem. Phys.* **2007**, *126*, No. 091101.
(38) Darancet, P.; Ferretti, A.; Mayou, D.; Olevano, V. Ab initio GW electron-electron interaction effects in Quantum Transport. *Phys. Rev. B: Condens. Matter Mater. Phys.* **2007**, *75*, No. 075102.
(39) Thoss, M.; Evers, F. Perspective: Theory of quantum transport in molecular junctions. *J. Chem. Phys.* **2018**, *148*, No. 030901.
(40) Sunjic, M.; Marusic, L. Dynamical effects in electron tunneling: Self-consistent semiclassical image potentials. *Phys. Rev. B: Condens. Matter Mater. Phys.* **1991**, *44*, 9092−9095.
(41) Rignanese, G. M.; Blase, X.; Louie, S. G. Quasiparticle effects on tunneling currents: A study of C2H4 adsorbed on the Si(001)-(2 × 1) surface. *Phys. Rev. Lett.* **2001**, *86*, 2110−2113.
(42) Dial, O. E.; Ashoori, R. C.; Pfeiffer, L. N.; West, K. W. Observations of plasmarons in a two-dimensional system: Tunneling measurements using time-domain capacitance spectroscopy. *Phys. Rev. B: Condens. Matter Mater. Phys.* **2012**, *85*, No. 081306.
(43) Aryasetiawan, F.; Gunnarsson, O. The GW method. *Rep. Prog. Phys.* **1998**, *61*, 237−312.
(44) Lischner, J.; Vigil-Fowler, D.; Louie, S. G. Physical origin of satellites in photoemission of doped graphene: An Ab initio GW plus cumulant study. *Phys. Rev. Lett.* **2013**, *110*, 146801.
(45) Golze, D.; Wilhelm, J.; Van Setten, M. J.; Rinke, P. Core-Level Binding Energies from GW: An Efficient Full-Frequency Approach within a Localized Basis. *J. Chem. Theory Comput.* **2018**, *14*, 4856−4869.
(46) Golze, D.; Dvorak, M.; Rinke, P. The GW Compendium: A Practical Guide to Theoretical Photoemission Spectroscopy. *Front. Chem.* **2019**, *7*, 377.
(47) Golze, D.; Keller, L.; Rinke, P. Accurate Absolute and Relative Core-Level Binding Energies From GW. *J. Phys. Chem. Lett.* **2020**, *11*, 1840−1847.
(48) Kühne, T. D.; Iannuzzi, M.; Del Ben, M.; Rybkin, V. V.; Seewald, P.; Stein, F.; Laino, T.; Khaliullin, R. Z.; Schütt, O.; Schiffmann, F.; Golze, D.; Wilhelm, J.; Chulkov, S.; Bani-Hashemian, M. H.; Weber, V.; Borstnik, U.; Taillefumier, M.; Jakobovits, A. S.; Lazzaro, A.; Pabst, H.; Müller, T.; Schade, R.; Guidon, M.; Andermatt, S.; Holmberg, N.; Schenter, G. K.; Hehn, A.; Bussy, A.;

https://dx.doi.org/10.1021/acs.jctc.0c00693
J. Chem. Theory Comput. 2020, 16, 7381−7399

Belleflamme, F.; Tabacchi, G.; Glöß, A.; Lass, M.; Bethune, I.; Mundy, C. J.; Plessl, C.; Watkins, M.; VandeVondele, J.; Krack, M.; Hutter, J. CP2K: An Electronic Structure and Molecular Dynamics Software Package − Quickstep: Efficient and Accurate Electronic Structure Calculations. *J. Chem. Phys.* **2020**, *152*, 194103.
(49) Luttinger, J. M.; Ward, J. C. On correlation effects in electron spectroscopies and the GW approximation. *Phys. Rev.* **1960**, *118*, 1417.
(50) Baym, G.; Kadanoff, L. P. Conservation laws and correlation functions. *Phys. Rev.* **1961**, *124*, 287−299.
(51) Hedin, L. New method for calculating the one-particle Green's function with application to the electron-gas problem. *Phys. Rev.* **1965**, *139*, A796.
(52) Onida, G.; Reining, L.; Rubio, A. Electronic excitations: density-functional versus many-body Green's-function approaches. *Rev. Mod. Phys.* **2002**, *74*, 601.
(53) Martin, R. M.; Reining, L.; Ceperley, D. M. *Interacting electrons*; Cambridge University Press, 2016.
(54) Reining, L. The GW approximation: content, successes and limitations. *Wiley Interdiscip. Rev.: Comput. Mol. Sci.* **2018**, *8*, No. e1344.
(55) Hybertsen, M. S.; Louie, S. G. Electron correlation in semiconductors and insulators: Band gaps and quasiparticle energies. *Phys. Rev. B: Condens. Matter Mater. Phys.* **1986**, *34*, 5390.
(56) Deslippe, J.; Samsonidze, G.; Strubbe, D. A.; Jain, M.; Cohen, M. L.; Louie, S. G. BerkeleyGW: A massively parallel computer package for the calculation of the quasiparticle and optical properties of materials and nanostructures. *Comput. Phys. Commun.* **2012**, *183*, 1269−1289.
(57) Pavlyukh, Y.; Stefanucci, G.; Van Leeuwen, R. Dynamically screened vertex correction to GW. *Phys. Rev. B: Condens. Matter Mater. Phys.* **2020**, *102*, 45121.
(58) Knight, J. W.; Wang, X.; Gallandi, L.; Dolgounitcheva, O.; Ren, X.; Ortiz, J. V.; Rinke, P.; Körzdörfer, T.; Marom, N. Accurate Ionization Potentials and Electron Affinities of Acceptor Molecules III: A Benchmark of GW Methods. *J. Chem. Theory Comput.* **2016**, *12*, 615−626.
(59) Salpeter, E. E.; Bethe, H. A. A relativistic equation for bound-state problems. *Phys. Rev.* **1951**, *84*, 1232−1242.
(60) Strinati, G. Application of the Green's functions method to the study of the optical properties of semiconductors. *La Riv. Del Nuovo Cim. Ser. 3* **1988**, *11*, 1−86.
(61) Gonze, X.; Beuken, J. M.; Caracas, R.; Detraux, F.; Fuchs, M.; Rignanese, G. M.; Sindic, L.; Verstraete, M.; Zerah, G.; Jollet, F.; Torrent, M.; Roy, A.; Mikami, M.; Ghosez, P.; Raty, J. Y.; Allan, D. C. First-principles computation of material properties: The ABINIT software project. *Comput. Mater. Sci.* **2002**, *25*, 478−492.
(62) Gonze, X.; Amadon, B.; Anglade, P. M.; Beuken, J. M.; Bottin, F.; Boulanger, P.; Bruneval, F.; Caliste, D.; Caracas, R.; Côté, M.; Deutsch, T.; Genovese, L.; Ghosez, P.; Giantomassi, M.; Goedecker, S.; Hamann, D. R.; Hermet, P.; Jollet, F.; Jomard, G.; Leroux, S.; Mancini, M.; Mazevet, S.; Oliveira, M. J.; Onida, G.; Pouillon, Y.; Rangel, T.; Rignanese, G. M.; Sangalli, D.; Shaltaf, R.; Torrent, M.; Verstraete, M. J.; Zerah, G.; Zwanziger, J. W. ABINIT: First-principles approach to material and nanosystem properties. *Comput. Phys. Commun.* **2009**, *180*, 2582−2615.
(63) Nguyen, H. V.; Pham, T. A.; Rocca, D.; Galli, G. Improving accuracy and efficiency of calculations of photoemission spectra within the many-body perturbation theory. *Phys. Rev. B: Condens. Matter Mater. Phys.* **2012**, *85*, No. 081101.
(64) Pham, T. A.; Nguyen, H. V.; Rocca, D.; Galli, G. GW calculations using the spectral decomposition of the dielectric matrix: Verification, validation, and comparison of methods. *Phys. Rev. B: Condens. Matter Mater. Phys.* **2013**, *87*, 155148.
(65) Kresse, G.; Furthmüller, J. Efficient iterative schemes for ab initio total-energy calculations using a plane-wave basis set. *Phys. Rev. B: Condens. Matter Mater. Phys.* **1996**, *54*, 11169−11186.
(66) Kresse, G.; Furthmüller, J. Efficiency of ab-initio total energy calculations for metals and semiconductors using a plane-wave basis set. *Comput. Mater. Sci.* **1996**, *6*, 15−50.
(67) Kresse, G.; Joubert, D. From ultrasoft pseudopotentials to the projector augmented-wave method. *Phys. Rev. B: Condens. Matter Mater. Phys.* **1999**, *59*, 1758−1775.
(68) Blum, V.; Gehrke, R.; Hanke, F.; Havu, P.; Havu, V.; Ren, X.; Reuter, K.; Scheffler, M. *The Fritz Haber Institute ab initio molecular simulations package (FHI-aims)*; 2009; http://www.fhi-berlin.mpg.de/aims.
(69) Blum, V.; Gehrke, R.; Hanke, F.; Havu, P.; Havu, V.; Ren, X.; Reuter, K.; Scheffler, M. Ab initio molecular simulations with numeric atom-centered orbitals. *Comput. Phys. Commun.* **2009**, *180*, 2175−2196.
(70) Bruneval, F.; Rangel, T.; Hamed, S. M.; Shao, M.; Yang, C.; Neaton, J. B. MOLGW 1: Many-body perturbation theory software for atoms, molecules, and clusters. *Comput. Phys. Commun.* **2016**, *208*, 149−161.
(71) Sangalli, D.; Ferretti, A.; Miranda, H.; Attaccalite, C.; Marri, I.; Cannuccia, E.; Melo, P.; Marsili, M.; Paleari, F.; Marrazzo, A.; Prandini, G.; Bonfà, P.; Atambo, M. O.; Affinito, F.; Palummo, M.; Molina-Sánchez, A.; Hogan, C.; Grüning, M.; Varsano, D.; Marini, A. Many-body perturbation theory calculations using the yambo code. *J. Phys.: Condens. Matter* **2019**, *31*, 325902.
(72) Schlipf, M.; Lambert, H.; Zibouche, N.; Giustino, F. STERNHEIMERGW: A program for calculating GW quasiparticle band structures and spectral functions without unoccupied states. *Comput. Phys. Commun.* **2020**, *247*, 106856.
(73) Blase, X.; Attaccalite, C.; Olevano, V. First-principles GW calculations for fullerenes, porphyrins, phtalocyanine, and other molecules of interest for organic photovoltaic applications. *Phys. Rev. B: Condens. Matter Mater. Phys.* **2011**, *83*, 115103.
(74) Faber, C.; Attaccalite, C.; Olevano, V.; Runge, E.; Blase, X. First-principles GW calculations for DNA and RNA nucleobases. *Phys. Rev. B: Condens. Matter Mater. Phys.* **2011**, *83*, 115123.
(75) Strange, M.; Rostgaard, C.; Häkkinen, H.; Thygesen, K. S. Self-consistent GW calculations of electronic transport in thiol- and amine-linked molecular junctions. *Phys. Rev. B: Condens. Matter Mater. Phys.* **2011**, *83*, 115108.
(76) Marom, N.; Caruso, F.; Ren, X.; Hofmann, O. T.; Körzdörfer, T.; Chelikowsky, J. R.; Rubio, A.; Scheffler, M.; Rinke, P. Benchmark of GW methods for azabenzenes. *Phys. Rev. B: Condens. Matter Mater. Phys.* **2012**, *86*, 245127.
(77) Baumeier, B.; Andrienko, D.; Rohlfing, M. Frenkel and charge-transfer excitations in donor-acceptor complexes from many-body green's functions theory. *J. Chem. Theory Comput.* **2012**, *8*, 2790−2795.
(78) Bruneval, F.; Marques, M. A. Benchmarking the starting points of the GW approximation for molecules. *J. Chem. Theory Comput.* **2013**, *9*, 324−329.
(79) Caruso, F.; Rohr, D. R.; Hellgren, M.; Ren, X.; Rinke, P.; Rubio, A.; Scheffler, M. Bond breaking and bond formation: How electron correlation is captured in many-body perturbation theory and density-functional theory. *Phys. Rev. Lett.* **2013**, *110*, 146403.
(80) Faber, C.; Boulanger, P.; Duchemin, I.; Attaccalite, C.; Blase, X. Many-body Green's function GW and Bethe-Salpeter study of the optical excitations in a paradigmatic model dipeptide. *J. Chem. Phys.* **2013**, *139*, 194308.
(81) Körbel, S.; Boulanger, P.; Duchemin, I.; Blase, X.; Marques, M. A.; Botti, S. Benchmark many-body GW and Bethe-Salpeter calculations for small transition metal molecules. *J. Chem. Theory Comput.* **2014**, *10*, 3934−3943.
(82) van Setten, M. J.; Caruso, F.; Sharifzadeh, S.; Ren, X.; Scheffler, M.; Liu, F.; Lischner, J.; Lin, L.; Deslippe, J. R.; Louie, S. G.; Yang, C.; Weigend, F.; Neaton, J. B.; Evers, F.; Rinke, P. GW100: Benchmarking G0W0 for Molecular Systems. *J. Chem. Theory Comput.* **2015**, *11*, 5665−5687.
(83) Rangel, T.; Hamed, S. M.; Bruneval, F.; Neaton, J. B. Evaluating the GW Approximation with CCSD(T) for Charged Excitations

https://dx.doi.org/10.1021/acs.jctc.0c00693
J. Chem. Theory Comput. 2020, 16, 7381−7399

Across the Oligoacenes. *J. Chem. Theory Comput.* **2016**, *12*, 2834−2842.
(84) Li, J.; D'Avino, G.; Duchemin, I.; Beljonne, D.; Blase, X. Combining the Many-Body GW Formalism with Classical Polarizable Models: Insights on the Electronic Structure of Molecular Solids. *J. Phys. Chem. Lett.* **2016**, *7*, 2814−2820.
(85) Duchemin, I.; Jacquemin, D.; Blase, X. Combining the GW formalism with the polarizable continuum model: A state-specific non-equilibrium approach. *J. Chem. Phys.* **2016**, *144*, 164106.
(86) Scherpelz, P.; Govoni, M.; Hamada, I.; Galli, G. Implementation and Validation of Fully Relativistic GW Calculations: Spin-Orbit Coupling in Molecules, Nanocrystals, and Solids. *J. Chem. Theory Comput.* **2016**, *12*, 3523−3544.
(87) Maggio, E.; Kresse, G. GW Vertex Corrected Calculations for Molecular Systems. *J. Chem. Theory Comput.* **2017**, *13*, 4765−4778.
(88) Hung, L.; Bruneval, F.; Baishya, K.; Öğüt, S. Benchmarking the GW Approximation and Bethe-Salpeter Equation for Groups IB and IIB Atoms and Monoxides. *J. Chem. Theory Comput.* **2017**, *13*, 2135−2146.
(89) Olsen, T.; Patrick, C. E.; Bates, J. E.; Ruzsinszky, A.; Thygesen, K. S. Beyond the RPA and GW methods with adiabatic xc-kernels for accurate ground state and quasiparticle energies. *Nat. Comput. Mater.* **2019**, *5*, 106.
(90) Bruneval, F. Assessment of the Linearized GW Density Matrix for Molecules. *J. Chem. Theory Comput.* **2019**, *15*, 4069−4078.
(91) Lewis, A. M.; Berkelbach, T. C. Vertex Corrections to the Polarizability Do Not Improve the GW Approximation for the Ionization Potential of Molecules. *J. Chem. Theory Comput.* **2019**, *15*, 2925−2932.
(92) Holzer, C.; Klopper, W. Ionized, electron-attached, and excited states of molecular systems with spin-orbit coupling: Two-component GW and Bethe-Salpeter implementations. *J. Chem. Phys.* **2019**, *150*, 204116.
(93) Cazzaniga, M.; Cargnoni, F.; Penconi, M.; Bossi, A.; Ceresoli, D. Ab Initio Many-Body Perturbation Theory Calculations of the Electronic and Optical Properties of Cyclometalated Ir(III) Complexes. *J. Chem. Theory Comput.* **2020**, *16*, 1188−1199.
(94) Caruso, F.; Dauth, M.; Van Setten, M. J.; Rinke, P. Benchmark of GW Approaches for the GW100 Test Set. *J. Chem. Theory Comput.* **2016**, *12*, 5076−5087.
(95) The notion of N^x always implies $O(N^x)$: That is, the function f, mapping the system size to the runtime of an algorithm, does not asymptotically grow faster than N^x.
(96) Shih, B. C.; Xue, Y.; Zhang, P.; Cohen, M. L.; Louie, S. G. Quasiparticle band gap of ZnO: High accuracy from the conventional G0W0 approach. *Phys. Rev. Lett.* **2010**, *105*, 146401.
(97) Nguyen, H. V.; Pham, T. A.; Rocca, D.; Galli, G. Improving accuracy and efficiency of calculations of photoemission spectra within the many-body perturbation theory. *Phys. Rev. B: Condens. Matter Mater. Phys.* **2012**, *85*, 081101.
(98) Del Ben, M.; da Jornada, F. H.; Canning, A.; Wichmann, N.; Raman, K.; Sasanka, R.; Yang, C.; Louie, S. G.; Deslippe, J. Large-scale GW calculations on pre-exascale HPC systems. *Comput. Phys. Commun.* **2019**, *235*, 187−195.
(99) Wilhelm, J.; Golze, D.; Talirz, L.; Hutter, J.; Pignedoli, C. A. Toward GW Calculations on Thousands of Atoms. *J. Phys. Chem. Lett.* **2018**, *9*, 306−312.
(100) Neuhauser, D.; Gao, Y.; Arntsen, C.; Karshenas, C.; Rabani, E.; Baer, R. Breaking the theoretical scaling limit for predicting quasiparticle energies: The stochastic GW approach. *Phys. Rev. Lett.* **2014**, *113*, 076402.
(101) Vlček, V.; Rabani, E.; Neuhauser, D.; Baer, R. Stochastic GW Calculations for Molecules. *J. Chem. Theory Comput.* **2017**, *13*, 4997−5003.
(102) Vlček, V.; Li, W.; Baer, R.; Rabani, E.; Neuhauser, D. Swift GW beyond 10,000 electrons using sparse stochastic compression. *Phys. Rev. B: Condens. Matter Mater. Phys.* **2018**, *98*, 075107.
(103) Umari, P.; Stenuit, G.; Baroni, S. GW quasiparticle spectra from occupied states only. *Phys. Rev. B: Condens. Matter Mater. Phys.* **2010**, *81*, 115104.
(104) Giustino, F.; Cohen, M. L.; Louie, S. G. GW method with the self-consistent Sternheimer equation. *Phys. Rev. B: Condens. Matter Mater. Phys.* **2010**, *81*, 115105.
(105) Lambert, H.; Giustino, F. Ab initio Sternheimer-GW method for quasiparticle calculations using plane waves. *Phys. Rev. B: Condens. Matter Mater. Phys.* **2013**, *88*, 075117.
(106) Bruneval, F. Optimized virtual orbital subspace for faster GW calculations in localized basis. *J. Chem. Phys.* **2016**, *145*, 234110.
(107) Govoni, M.; Galli, G. Large Scale GW Calculations. *J. Chem. Theory Comput.* **2015**, *11*, 2680−2696.
(108) Rostgaard, C.; Jacobsen, K. W.; Thygesen, K. S. Fully self-consistent GW calculations for molecules. *Phys. Rev. B: Condens. Matter Mater. Phys.* **2010**, *81*, 085103.
(109) Shao, M. Y.; Lin, L.; Yang, C.; Liu, F.; Da Jornada, F. H.; Deslippe, J.; Louie, S. G. Low rank approximation in G0W0 calculations. *Sci. China Math.* **2016**, *59*, 1593−1612.
(110) Klimeš, J.; Kaltak, M.; Kresse, G. Predictive GW calculations using plane waves and pseudopotentials. *Phys. Rev. B: Condens. Matter Mater. Phys.* **2014**, *90*, 075125.
(111) Riemelmoser, S.; Kaltak, M.; Kresse, G. Plane wave basis set correction methods for RPA correlation energies. *J. Chem. Phys.* **2020**, *152*, 134103.
(112) Loos, P. F.; Pradines, B.; Scemama, A.; Giner, E.; Toulouse, J. Density-Based Basis-Set Incompleteness Correction for GW Methods. *J. Chem. Theory Comput.* **2020**, *16*, 1018−1028.
(113) Helgaker, T.; Jorgensen, P.; Olsen, J. *Molecular electronic-structure theory*; John Wiley & Sons, 2014.
(114) Billingsley, F. P.; Bloor, J. E. Limited expansion of diatomic overlap (LEDO): A Near-accurate approximate Ab Initio LCAO MO Method. I. Theory and preliminary investigations. *J. Chem. Phys.* **1971**, *55*, 5178−5190.
(115) Baerends, E. J.; Ellis, D. E.; Ros, P. Self-consistent molecular Hartree—Fock—Slater calculations I. The computational procedure. *Chem. Phys.* **1973**, *2*, 41−51.
(116) Whitten, J. L. Coulombic potential energy integrals and approximations. *J. Chem. Phys.* **1973**, *58*, 4496−4501.
(117) Sambe, H.; Felton, R. H. A new computational approach to Slater's SCF-X α equation. *J. Chem. Phys.* **1975**, *62*, 1122−1126.
(118) Dunlap, B. I.; Connolly, J. W.; Sabin, J. R. On some approximations in applications of Xα theory. *J. Chem. Phys.* **1979**, *71*, 3396−3402.
(119) Dunlap, B. I.; Connolly, J. W.; Sabin, J. R. On first-row diatomic molecules and local density models. *J. Chem. Phys.* **1979**, *71*, 4993−4999.
(120) Vahtras, O.; Almlöf, J.; Feyereisen, M. W. Integral approximations for LCAO-SCF calculations. *Chem. Phys. Lett.* **1993**, *213*, 514−518.
(121) Feyereisen, M.; Fitzgerald, G.; Komornicki, A. Use of approximate integrals in ab initio theory. An application in MP2 energy calculations. *Chem. Phys. Lett.* **1993**, *208*, 359−363.
(122) Kendall, R. A.; Früchtl, H. A. The impact of the resolution of the identity approximate integral method on modern ab initio algorithm development. *Theor. Chem. Acc.* **1997**, *97*, 158−163.
(123) Dunlap, B. I. Robust and variational fitting: Removing the four-center integrals from center stage in quantum chemistry. *J. Mol. Struct.: THEOCHEM* **2000**, *529*, 37−40.
(124) Dunlap, B. I. Robust and variational fitting. *Phys. Chem. Chem. Phys.* **2000**, *2*, 2113−2116.
(125) Weigend, F. Accurate Coulomb-fitting basis sets for H to Rn. *Phys. Chem. Chem. Phys.* **2006**, *8*, 1057−1065.
(126) Dunlap, B. I.; Rösch, N.; Trickey, S. B. Variational fitting methods for electronic structure calculations. *Mol. Phys.* **2010**, *108*, 3167−3180.
(127) Beebe, N. H.; Linderberg, J. Simplifications in the generation and transformation of two-electron integrals in molecular calculations. *Int. J. Quantum Chem.* **1977**, *12*, 683−705.

https://dx.doi.org/10.1021/acs.jctc.0c00693
J. Chem. Theory Comput. 2020, 16, 7381−7399

(128) Koch, H.; Sánchez De Merás, A.; Pedersen, T. B. Reduced scaling in electronic structure calculations using Cholesky decompositions. *J. Chem. Phys.* **2003**, *118*, 9481−9484.
(129) Aquilante, F.; Lindh, R.; Bondo Pedersen, T. Unbiased auxiliary basis sets for accurate two-electron integral approximations. *J. Chem. Phys.* **2007**, *127*, 114107.
(130) Boman, L.; Koch, H.; Sánchez De Merás, A. Method specific Cholesky decomposition: Coulomb and exchange energies. *J. Chem. Phys.* **2008**, *129*, 134107.
(131) Aquilante, F.; Gagliardi, L.; Pedersen, T. B.; Lindh, R. Atomic Cholesky decompositions: A route to unbiased auxiliary basis sets for density fitting approximation with tunable accuracy and efficiency. *J. Chem. Phys.* **2009**, *130*, 154107.
(132) Foerster, D.; Koval, P.; Sanchez-Portal, D. An O(N3) implementation of Hedins GW approximation for molecules. *J. Chem. Phys.* **2011**, *135*, No. 074105.
(133) Ke, S. H. All-electron GW methods implemented in molecular orbital space: Ionization energy and electron affinity of conjugated molecules. *Phys. Rev. B: Condens. Matter Mater. Phys.* **2011**, *84*, 205415.
(134) Ren, X.; Rinke, P.; Blum, V.; Wieferink, J.; Tkatchenko, A.; Sanfilippo, A.; Reuter, K.; Scheffler, M. Resolution-of-identity approach to Hartree-Fock, hybrid density functionals, RPA, MP2 and GW with numeric atom-centered orbital basis functions. *New J. Phys.* **2012**, *14*, No. 053020.
(135) van Setten, M. J.; Weigend, F.; Evers, F. The GW-method for quantum chemistry applications: Theory and implementation. *J. Chem. Theory Comput.* **2013**, *9*, 232−246.
(136) Caruso, F.; Rinke, P.; Ren, X.; Rubio, A.; Scheffler, M. Self-consistent GW: All-electron implementation with localized basis functions. *Phys. Rev. B: Condens. Matter Mater. Phys.* **2013**, *88*, 075105.
(137) Kaplan, F.; Harding, M. E.; Seiler, C.; Weigend, F.; Evers, F.; Van Setten, M. J. Quasi-Particle Self-Consistent GW for Molecules. *J. Chem. Theory Comput.* **2016**, *12*, 2528−2541.
(138) Krause, K.; Klopper, W. Implementation of the Bethe-Salpeter equation in the TURBOMOLE program. *J. Comput. Chem.* **2017**, *38*, 383−388.
(139) Tirimbò, G.; Sundaram, V.; Çaylak, O.; Scharpach, W.; Sijen, J.; Junghans, C.; Brown, J.; Ruiz, F. Z.; Renaud, N.; Wehner, J.; Baumeier, B. Excited-state electronic structure of molecules using many-body Green's functions: Quasiparticles and electron-hole excitations with VOTCA-XTP. *J. Chem. Phys.* **2020**, *152*, 114103.
(140) Watson, M. A.; Handy, N. C.; Cohen, A. J. Density functional calculations, using Slater basis sets, with exact exchange. *J. Chem. Phys.* **2003**, *119*, 6475−6481.
(141) Polly, R.; Werner, H. J.; Manby, F. R.; Knowles, P. J. Fast Hartree-Fock theory using local density fitting approximations. *Mol. Phys.* **2004**, *102*, 2311−2321.
(142) Sodt, A.; Subotnik, J. E.; Head-Gordon, M. Linear scaling density fitting. *J. Chem. Phys.* **2006**, *125*, 194109.
(143) Sodt, A.; Head-Gordon, M. Hartree-Fock exchange computed using the atomic resolution of the identity approximation. *J. Chem. Phys.* **2008**, *128*, 104106.
(144) Almlöf, J. Elimination of energy denominators in Møller-Plesset perturbation theory by a Laplace transform approach. *Chem. Phys. Lett.* **1991**, *181*, 319−320.
(145) Häser, M.; Almlöf, J. Laplace transform techniques in Møller-Plesset perturbation theory. *J. Chem. Phys.* **1992**, *96*, 489−494.
(146) Häser, M. Møller-Plesset (MP2) perturbation theory for large molecules. *Theor. Chim. Acta* **1993**, *87*, 147−173.
(147) Rojas, H. N.; Godby, R. W.; Needs, R. J. Space-Time Method for Ab Initio Calculations ofSelf-Energies and Dielectric Response Functions of Solids. *Phys. Rev. Lett.* **1995**, *74*, 1827−1831.
(148) Rieger, M. M.; Steinbeck, L.; White, I. D.; Rojas, H. N.; Godby, R. W. GW space-time method for the self-energy of large systems. *Comput. Phys. Commun.* **1999**, *117*, 211−228.
(149) Fonseca Guerra, C.; Snijders, J. G.; te Velde, G.; Baerends, E. J. Towards an order-N DFT method. *Theor. Chem. Acc.* **1998**, *99*, 391−403.
(150) Krykunov, M.; Ziegler, T.; Van Lenthe, E. Hybrid density functional calculations of nuclear magnetic shieldings using slater-type orbitals and the zeroth- order regular approximation. *Int. J. Quantum Chem.* **2009**, *109*, 1676−1683.
(151) Merlot, P.; Kjærgaard, T.; Helgaker, T.; Lindh, R.; Aquilante, F.; Reine, S.; Pedersen, T. B. Attractive electron-electron interactions within robust local fitting approximations. *J. Comput. Chem.* **2013**, *34*, 1486−1496.
(152) Hollman, D. S.; Schaefer, H. F.; Valeev, E. F. Semi-exact concentric atomic density fitting: Reduced cost and increased accuracy compared to standard density fitting. *J. Chem. Phys.* **2014**, *140*, No. 064109.
(153) Mejía-Rodríguez, D.; Köster, A. M. Robust and efficient variational fitting of Fock exchange. *J. Chem. Phys.* **2014**, *141*, 124114.
(154) Manzer, S. F.; Epifanovsky, E.; Head-Gordon, M. Efficient implementation of the pair atomic resolution of the identity approximation for exact exchange for hybrid and range-separated density functionals. *J. Chem. Theory Comput.* **2015**, *11*, 518−527.
(155) Lewis, C. A.; Calvin, J. A.; Valeev, E. F. Clustered Low-Rank Tensor Format: Introduction and Application to Fast Construction of Hartree-Fock Exchange. *J. Chem. Theory Comput.* **2016**, *12*, 5868−5880.
(156) Hollman, D. S.; Schaefer, H. F.; Valeev, E. F. Fast construction of the exchange operator in an atom-centred basis with concentric atomic density fitting. *Mol. Phys.* **2017**, *115*, 2065−2076.
(157) Lin, P.; Ren, X.; He, L. Hybrid Functional Calculations with Numerical Atomic Orbitals On the Accuracy of Localized Resolution-of-the-Identity in Periodic Hybrid Functional Calculations with Numerical Atomic Orbitals. *J. Phys. Chem. Lett.* **2020**, *11*, 3082−3088.
(158) Rebolini, E.; Izsák, R.; Reine, S. S.; Helgaker, T.; Pedersen, T. B. Comparison of Three Efficient Approximate Exact-Exchange Algorithms: The Chain-of-Spheres Algorithm, Pair-Atomic Resolution-of-the-Identity Method, and Auxiliary Density Matrix Method. *J. Chem. Theory Comput.* **2016**, *12*, 3514−3522.
(159) Wirz, L. N.; Reine, S. S.; Pedersen, T. B. On Resolution-of-the-Identity Electron Repulsion Integral Approximations and Variational Stability. *J. Chem. Theory Comput.* **2017**, *13*, 4897−4906.
(160) Ihrig, A. C.; Wieferink, J.; Zhang, I. Y.; Ropo, M.; Ren, X.; Rinke, P.; Scheffler, M.; Blum, V. Accurate localized resolution of identity approach for linear-scaling hybrid density functionals and for many-body perturbation theory. *New J. Phys.* **2015**, *17*, No. 093020.
(161) Tew, D. P. Communication: Quasi-robust local density fitting. *J. Chem. Phys.* **2018**, *148*, No. 011102.
(162) Förster, A.; Franchini, M.; van Lenthe, E.; Visscher, L. A Quadratic Pair Atomic Resolution of the Identity Based SOS-AO-MP2 Algorithm Using Slater Type Orbitals. *J. Chem. Theory Comput.* **2020**, *16*, 875−891.
(163) Förster, A.; Visscher, L. Double hybrid DFT calculations with Slater type orbitals. *J. Comput. Chem.* **2020**, *41*, 1660−1684.
(164) Kaltak, M.; Klimeš, J.; Kresse, G. Low scaling algorithms for the random phase approximation: Imaginary time and laplace transformations. *J. Chem. Theory Comput.* **2014**, *10*, 2498−2507.
(165) Kaltak, M.; Klimeš, J.; Kresse, G. Cubic scaling algorithm for the random phase approximation: Self-interstitials and vacancies in Si. *Phys. Rev. B: Condens. Matter Mater. Phys.* **2014**, *90*, 054115.
(166) Liu, P.; Kaltak, M.; Klimeš, J.; Kresse, G. Cubic scaling GW: Towards fast quasiparticle calculations. *Phys. Rev. B: Condens. Matter Mater. Phys.* **2016**, *94*, 165109.
(167) Grumet, M.; Liu, P.; Kaltak, M.; Klimeš, J.; Kresse, G. Beyond the quasiparticle approximation: Fully self-consistent GW calculations. *Phys. Rev. B: Condens. Matter Mater. Phys.* **2018**, *98*, 155143.
(168) Wilhelm, J.; Seewald, P.; Del Ben, M.; Hutter, J. Large-Scale Cubic-Scaling Random Phase Approximation Correlation Energy Calculations Using a Gaussian Basis. *J. Chem. Theory Comput.* **2016**, *12*, 5851−5859.

https://dx.doi.org/10.1021/acs.jctc.0c00693
J. Chem. Theory Comput. 2020, 16, 7381−7399

(169) Duchemin, I.; Blase, X. Separable resolution-of-the-identity with all-electron Gaussian bases: Application to cubic-scaling RPA. *J. Chem. Phys.* **2019**, *150*, 174120.
(170) Van Schilfgaarde, M.; Kotani, T.; Faleev, S. Quasiparticle self-consistent GW theory. *Phys. Rev. Lett.* **2006**, *96*, 226402.
(171) Kotani, T.; Van Schilfgaarde, M.; Faleev, S. V. Quasiparticle self-consistent GW method: A basis for the independent-particle approximation. *Phys. Rev. B: Condens. Matter Mater. Phys.* **2007**, *76*, 165106.
(172) te Velde, G.; Bickelhaupt, F. M.; Baerends, E. J.; Fonseca Guerra, C.; van Gisbergen, S.; Snijders, J. G.; Ziegler, T. Chemistry with ADF. *J. Comput. Chem.* **2001**, *22*, 931−967.
(173) Baerends, E.; Ziegler, T.; Atkins, A.; Autschbach, J.; Baseggio, O.; Bashford, D.; Bérces, A.; Bickelhaupt, F.; Bo, C.; Boerrigter, P.; Cavallo, L.; Daul, C.; Chong, D.; Chulhai, D.; Deng, L.; Dickson, R.; Dieterich, J.; Ellis, D.; van Faassen, M.; Fan, L.; Fischer, T.; Förster, A.; Guerra, C. F.; Franchini, M.; Ghysels, A.; Giammona, A.; van Gisbergen, S.; Goez, A.; Götz, A.; Groeneveld, J.; Gritsenko, O.; Grüning, M.; Gusarov, S.; Harris, F.; van den Hoek, P.; Hu, Z.; Jacob, C.; Jacobsen, H.; Jensen, L.; Joubert, L.; Kaminski, J.; van Kessel, G.; König, C.; Kootstra, F.; Kovalenko, A.; Krykunov, M.; van Lenthe, E.; McCormack, D.; Michalak, A.; Mitoraj, M.; Morton, S.; Neugebauer, J.; Nicu, V.; Noodleman, L.; Osinga, V.; Patchkovskii, S.; Pavanello, M.; Peeples, C.; Philipsen, P.; Post, D.; Pye, C.; Ramanantoanina, H.; Ramos, P.; Ravenek, W.; Rodríguez, J.; Ros, P.; Rüger, R.; Schipper, P.; Schlüns, D.; van Schoot, H.; Schreckenbach, G.; Seldenthuis, J.; Seth, M.; Snijders, J.; Solà, M.; Stener, M.; Swart, M.; Swerhone, D.; Tognetti, V.; te Velde, G.; Vernooijs, P.; Versluis, L.; Visscher, L.; Visser, O.; Wang, F.; Wesolowski, T.; van Wezenbeek, E.; Wiesenekker, G.; Wolff, S.; Woo, T.; Yakovlev, A. *ADF2019.3, SCM, Theoretical Chemistry*; Vrije Universiteit: Amsterdam, The Netherlands; https://www.scm.com.
(174) Stan, A.; Dahlen, N. E.; Van Leeuwen, R. Levels of self-consistency in the GW approximation. *J. Chem. Phys.* **2009**, *130*, 114105.
(175) Cancés, E.; Gontier, D.; Stoltz, G. A mathematical analysis of the GW0 method for computing electronic excited energies of molecules. *Rev. Math. Phys.* **2016**, *28*, 1650008.
(176) Han, X. J.; Liao, H. J.; Xie, H. D.; Huang, R. Z.; Meng, Z. Y.; Xiang, T. Analytic Continuation with Padé Decomposition. *Chin. Phys. Lett.* **2017**, *34*, 077102.
(177) Surján, P. R. The MP2 energy as a functional of the Hartree-Fock density matrix. *Chem. Phys. Lett.* **2005**, *406*, 318−320.
(178) Starke, R.; Kresse, G. Self-consistent Green function equations and the hierarchy of approximations for the four-point propagator. *Phys. Rev. B: Condens. Matter Mater. Phys.* **2012**, *85*, 075119.
(179) Schutski, R.; Zhao, J.; Henderson, T. M.; Scuseria, G. E. Tensor-structured coupled cluster theory. *J. Chem. Phys.* **2017**, *147*, 184113.
(180) Kohn, W. Density functional and density matrix method scaling linearly with the number of atoms. *Phys. Rev. Lett.* **1996**, *76*, 3168−3171.
(181) Baer, R.; Head-Gordon, M. Sparsity of the density matrix in kohn-sham density functional theory and an assessment of linear system-size scaling methods. *Phys. Rev. Lett.* **1997**, *79*, 3962−3965.
(182) Goedecker, S. Linear scaling electronic structure methods. *Rev. Mod. Phys.* **1999**, *71*, 1085−1123.
(183) Schindlmayr, A. Decay properties of the one-particle Green function in real space and imaginary time. *Phys. Rev. B: Condens. Matter Mater. Phys.* **2000**, *62*, 12573−12576.
(184) Zienau, J.; Clin, L.; Doser, B.; Ochsenfeld, C. Cholesky-decomposed densities in laplace-based second-order møller-plesset perturbation theory. *J. Chem. Phys.* **2009**, *130*, 204112.
(185) Maurer, S. A.; Kussmann, J.; Ochsenfeld, C. Communication: A reduced scaling J-engine based reformulation of SOS-MP2 using graphics processing units. *J. Chem. Phys.* **2014**, *141*, No. 051106.
(186) Maurer, S. A.; Clin, L.; Ochsenfeld, C. Cholesky-decomposed density MP2 with density fitting: Accurate MP2 and double-hybrid DFT energies for large systems. *J. Chem. Phys.* **2014**, *140*, 224112.
(187) Schurkus, H. F.; Ochsenfeld, C. Communication: An effective linear-scaling atomic-orbital reformulation of the random-phase approximation using a contracted double-Laplace transformation. *J. Chem. Phys.* **2016**, *144*, No. 031101.
(188) Luenser, A.; Schurkus, H. F.; Ochsenfeld, C. Vanishing-Overhead Linear-Scaling Random Phase Approximation by Cholesky Decomposition and an Attenuated Coulomb-Metric. *J. Chem. Theory Comput.* **2017**, *13*, 1647−1655.
(189) Graf, D.; Beuerle, M.; Schurkus, H. F.; Luenser, A.; Savasci, G.; Ochsenfeld, C. Accurate and Efficient Parallel Implementation of an Effective Linear-Scaling Direct Random Phase Approximation Method. *J. Chem. Theory Comput.* **2018**, *14*, 2505−2515.
(190) Graf, D.; Beuerle, M.; Ochsenfeld, C. Low-Scaling Self-Consistent Minimization of a Density Matrix Based Random Phase Approximation Method in the Atomic Orbital Space. *J. Chem. Theory Comput.* **2019**, *15*, 4468−4477.
(191) Rudberg, E.; Rubensson, E. H.; Sałek, P. Hartree-Fock calculations with linearly scaling memory usage. *J. Chem. Phys.* **2008**, *128*, 184106.
(192) Rudberg, E.; Rubensson, E. H.; Sałek, P. Kohn-sham density functional theory electronic structure calculations with linearly scaling computational time and memory usage. *J. Chem. Theory Comput.* **2011**, *7*, 340−350.
(193) Vandevondele, J.; Borštnik, U.; Hutter, J. Linear scaling self-consistent field calculations with millions of atoms in the condensed phase. *J. Chem. Theory Comput.* **2012**, *8*, 3565−3573.
(194) Eichkorn, K.; Treutler, O.; Öhm, H.; Häser, M.; Ahlrichs, R. Auxiliary basis sets to approximate Coulomb potentials. *Chem. Phys. Lett.* **1995**, *240*, 283−290.
(195) Klahn, B.; Bingel, W. A. Completeness and Linear Independence of Basis Sets Used in Quantum Chemistry. *Int. J. Quantum Chem.* **1977**, *11*, 943−957.
(196) Löwdin, P. O. Group algebra, convolution algebra, and applications to quantum mechanics. *Rev. Mod. Phys.* **1967**, *39*, 259−287.
(197) Kudin, K. N.; Scuseria, G. E. Linear-scaling density-functional theory with Gaussian orbitals and periodic boundary conditions: Efficient evaluation of energy and forces via the fast multipole method. *Phys. Rev. B: Condens. Matter Mater. Phys.* **2000**, *61*, 16440−16453.
(198) Suhai, S.; Bagus, P. S.; Ladik, J. An error analysis for Hartree-Fock crystal orbital calculations. *Chem. Phys.* **1982**, *68*, 467−471.
(199) Kudin, K. N.; Scuseria, G. E.; Cancès, E. A black-box self-consistent field convergence algorithm: One step closer. *J. Chem. Phys.* **2002**, *116*, 8255−8261.
(200) Lehtola, S.; Blockhuys, F.; Van Alsenoy, C. An overview of self-consistent field calculations within finite basis sets. *Molecules* **2020**, *25*, 1218.
(201) Schipper, P. R.; Gritsenko, O. V.; Van Gisbergen, S. J.; Baerends, E. J. Molecular calculations of excitation energies and (hyper)polarizabilities with a statistical average of orbital model exchange-correlation potentials. *J. Chem. Phys.* **2000**, *112*, 1344−1352.
(202) De Jong, G. T.; Visscher, L. Using the locality of the small-component density in molecular Dirac-Hartree-Fock calculations. *Theor. Chem. Acc.* **2002**, *107*, 304−308.
(203) Takatsuka, A.; Ten-no, S.; Hackbusch, W. Minimax approximation for the decomposition of energy denominators in Laplace-transformed MøllerPlesset perturbation theories. *J. Chem. Phys.* **2008**, *129*, No. 044112.
(204) Helmich-Paris, B.; Visscher, L. Improvements on the minimax algorithm for the Laplace transformation of orbital energy denominators. *J. Comput. Phys.* **2016**, *321*, 927−931.
(205) Levenberg, K. A method for the solution of certain non-linear problems in least squares. *Q. Appl. Math.* **1944**, *2*, 164−168.
(206) Marquardt, D. W. An algorithm for least-squares estimation of nonlinear parameters. *J. Soc. Ind. Appl. Math.* **1963**, *11*, 431−441.
(207) Source code available on https://github.com/bhelmichparis/laplace-minimax.

https://dx.doi.org/10.1021/acs.jctc.0c00693
J. Chem. Theory Comput. 2020, 16, 7381−7399

(208) Vidberg, H. J.; Serene, J. W. Solving the Eliashberg equations by means of N-point Padé approximants. *J. Low Temp. Phys.* **1977**, *29*, 179−192.
(209) Wilhelm, J.; Del Ben, M.; Hutter, J. GW in the Gaussian and Plane Waves Scheme with Application to Linear Acenes. *J. Chem. Theory Comput.* **2016**, *12*, 3623−3635.
(210) Govoni, M.; Galli, G. GW100: Comparison of Methods and Accuracy of Results Obtained with the WEST Code. *J. Chem. Theory Comput.* **2018**, *14*, 1895−1909.
(211) Franchini, M.; Philipsen, P. H. T.; Van Lenthe, E.; Visscher, L. Accurate Coulomb potentials for periodic and molecular systems through density fitting. *J. Chem. Theory Comput.* **2014**, *10*, 1994−2004.
(212) Ernzerhof, M.; Scuseria, G. E. Assessment of the PerdewBurkeErnzerhof exchange-correlation functional. *J. Chem. Phys.* **1999**, *110*, 5029.
(213) Adamo, C.; Barone, V. Toward reliable density functional methods without adjustable parameters: The PBE0 model. *J. Chem. Phys.* **1999**, *110*, 6158−6170.
(214) Stuke, A.; Kunkel, C.; Golze, D.; Todorović, M.; Margraf, J. T.; Reuter, K.; Rinke, P.; Oberhofer, H. Atomic structures and orbital energies of 61,489 crystal-forming organic molecules. *Sci. Data* **2020**, *7*, 58.
(215) Data downloaded from the website of the GW100 project by Van Setten et al. https://gw100.wordpress.com (accessed 2020-06-10).
(216) Chong, D. P.; Van Lenthe, E.; Van Gisbergen, S.; Baerends, E. J. Even-tempered slater-type orbitals revisited: From hydrogen to krypton. *J. Comput. Chem.* **2004**, *25*, 1030−1036.
(217) van Lenthe, E.; Baerends, J. E. Optimized Slater-type basis sets for the elements 1−118. *J. Comput. Chem.* **2003**, *24*, 1142−1156.
(218) Details of the composition of the fit sets can be found in the Supporting Information of our recent work.[162]
(219) The individual numbers of points can differ. This is due to the fact that we adjust the grid sizes at the runtime to match a certain error parameter. Thus, for many systems, the number of points will actually be smaller than 18, since the imaginary time and frequency integrals are already converged with a smaller number of points.
(220) Van Lenthe, E.; Baerends, E. J.; Snijders, J. G. Relativistic regular two-component hamiltonians. *J. Chem. Phys.* **1993**, *99*, 4597.
(221) Van Lenthe, E.; Baerends, E. J.; Snijders, J. G. Relativistic total energy using regular approximations. *J. Chem. Phys.* **1994**, *101*, 9783−9792.
(222) Van Lenthe, E.; Snijders, J. G.; Baerends, E. J. The zero-order regular approximation for relativistic effects: The effect of spin-orbit coupling in closed shell molecules. *J. Chem. Phys.* **1996**, *105*, 6505−6516.
(223) Van Lenthe, E.; Ehlers, A.; Baerends, J. E. Geometry optimizations in the zero order regular approximation for relativistic effects. *J. Chem. Phys.* **1999**, *110*, 8943−8953.
(224) Payne, M. C.; Teter, M. P.; Allan, D. C.; Arias, T. A.; Joannopoulos, J. D. Iterative minimization techniques for ab initio total-energy molecular dynamics and conjugate gradients calculations: *Rev. Mod. Phys.* **1992**, *64*, 1045−1097.
(225) Varga, K.; Zhang, Z.; Pantelides, S. T. Lagrange functions": A family of powerful basis sets for real-space order-N electronic structure calculations. *Phys. Rev. Lett.* **2004**, *93*, 176403.
(226) Maggio, E.; Liu, P.; Van Setten, M. J.; Kresse, G. GW100: A Plane Wave Perspective for Small Molecules. *J. Chem. Theory Comput.* **2017**, *13*, 635−648.
(227) Gao, W.; Chelikowsky, J. R. Real-Space Based Benchmark of G0W0 Calculations on GW100: Effects of Semicore Orbitals and Orbital Reordering. *J. Chem. Theory Comput.* **2019**, *15*, 5299−5307.
(228) These reference values have been calculated by Tiago and Chelikowsky with the nanoGW[229] package, which implements *GW* in RS and with a full frequency treatment. The calculations have been performed using KS orbitals and energies calculated with the PARSEC code.[246,247] For details, we refer to the original work.[227]
(229) Tiago, M. L.; Chelikowsky, J. R. Optical excitations in organic molecules, clusters, and defects studied by first-principles Green's function methods. *Phys. Rev. B: Condens. Matter Mater. Phys.* **2006**, *73*, 205334.
(230) Balasubramani, S. G.; Chen, G. P.; Coriani, S.; Diedenhofen, M.; Frank, M. S.; Franzke, Y. J.; Furche, F.; Grotjahn, R.; Harding, M. E.; Hättig, C.; Hellweg, A.; Helmich-Paris, B.; Holzer, C.; Huniar, U.; Kaupp, M.; Khah, A. M.; Khani, S. K.; Müller, T.; Mack, F.; Nguyen, B. D.; Parker, S. M.; Perlt, E.; Rappoport, D.; Reiter, K.; Roy, S.; Rückert, M.; Schmitz, G.; Sierka, M.; Tapavicza, E.; Tew, D. P.; van Wüllen, C.; Voora, V. K.; Weigend, F.; Wodynski, A.; Yu, J. M. TURBOMOLE: Modular program suite for ab initio quantum-chemical and condensed-matter simulations. *J. Chem. Phys.* **2020**, *152*, 184107.
(231) Pritchard, B. P.; Altarawy, D.; Didier, B.; Gibson, T. D.; Windus, T. L. New Basis Set Exchange: An Open, Up-to-Date Resource for the Molecular Sciences Community. *J. Chem. Inf. Model.* **2019**, *59*, 4814−4820.
(232) Boulanger, P.; Jacquemin, D.; Duchemin, I.; Blase, X. Fast and accurate electronic excitations in cyanines with the many-body bethe-salpeter approach. *J. Chem. Theory Comput.* **2014**, *10*, 1212−1218.
(233) Faber, C.; Boulanger, P.; Attaccalite, C.; Cannuccia, E.; Duchemin, I.; Deutsch, T.; Blase, X. Exploring approximations to the GW self-energy ionic gradients. *Phys. Rev. B: Condens. Matter Mater. Phys.* **2015**, *91*, 155109.
(234) Jacquemin, D.; Duchemin, I.; Blase, X. Benchmarking the Bethe-Salpeter Formalism on a Standard Organic Molecular Set. *J. Chem. Theory Comput.* **2015**, *11*, 3290−3304.
(235) Bruneval, F.; Hamed, S. M.; Neaton, J. B. A systematic benchmark of the ab initio Bethe-Salpeter equation approach for low-lying optical excitations of small organic molecules. *J. Chem. Phys.* **2015**, *142*, 244101.
(236) Harris, C. R.; Millman, K. J.; van der Walt, S. J.; Gommers, R.; Virtanen, P.; Cournapeau, D.; Wieser, E.; Taylor, J.; Berg, S.; Smith, N. J.; Kern, R.; Picus, M.; Hoyer, S.; van Kerkwijk, M. H.; Brett, M.; Haldane, A.; del Río, J. F.; Wiebe, M.; Peterson, P.; Gérard-Marchant, P.; Sheppard, K.; Reddy, T.; Weckesser, W.; Abbasi, H.; Gohlke, C.; Oliphant, T. E. Array Programming with NumPy. *Nature* **2020**, *585*, 357−362.
(237) The structures of the water clusters have been downloaded from the website of the ERGO program;[248] http://www.ergoscf.org (accessed 2020-05-19).
(238) Lange, M. F.; Berkelbach, T. C. On the Relation between Equation-of-Motion Coupled-Cluster Theory and the GW Approximation. *J. Chem. Theory Comput.* **2018**, *14*, 4224−4236.
(239) Weigend, F.; Häser, M.; Patzelt, H.; Ahlrichs, R. RI-MP2: Optimized auxiliary basis sets and demonstration of efficiency. *Chem. Phys. Lett.* **1998**, *294*, 143−152.
(240) Hättig, C.; Weigend, F. CC2 excitation energy calculations on large molecules using the resolution of the identity approximation. *J. Chem. Phys.* **2000**, *113*, 5154−5161.
(241) Weigend, F.; Köhn, A.; Hättig, C. Efficient use of the correlation consistent basis sets in resolution of the identity MP2 calculations. *J. Chem. Phys.* **2002**, *116*, 3175−3183.
(242) Werner, H. J.; Manby, F. R.; Knowles, P. J. Fast linear scaling second-order Møller-Plesset perturbation theory (MP2) using local and density fitting approximations. *J. Chem. Phys.* **2003**, *118*, 8149−8160.
(243) Schütz, M.; Manby, F. R. Linear scaling local coupled cluster theory with density fitting. Part I: 4-external integrals. *Phys. Chem. Chem. Phys.* **2003**, *5*, 3349−3358.
(244) Hättig, C. Geometry optimizations with the coupled-cluster model CC2 using the resolution-of-the-identity approximation. *J. Chem. Phys.* **2003**, *118*, 7751−7761.
(245) Klopper, W.; Manby, F. R.; Ten-No, S.; Valeev, E. F. R12 methods in explicitly correlated molecular electronic structure theory. *Int. Rev. Phys. Chem.* **2006**, *25*, 427−468.

https://dx.doi.org/10.1021/acs.jctc.0c00693
J. Chem. Theory Comput. 2020, 16, 7381−7399

(246) Chelikowsky, J. R.; Troullier, N.; Saad, Y. Finite-difference-pseudopotential method: Electronic structure calculations without a basis. *Phys. Rev. Lett.* **1994**, *72*, 1240−1243.
(247) Kronik, L.; Makmal, A.; Tiago, M. L.; Alemany, M. M.; Jain, M.; Huang, X.; Saad, Y.; Chelikowsky, J. R. PARSEC - The pseudopotential algorithm for real-space electronic structure calculations: Recent advances and novel applications to nano-structures. *Phys. Status Solidi B* **2006**, *243*, 1063−1079.
(248) Rudberg, E.; Rubensson, E. H.; Sałek, P.; Kruchinina, A. Ergo: An open-source program for linear-scaling electronic structure calculations. *SoftwareX* **2018**, *7*, 107−111.

https://dx.doi.org/10.1021/acs.jctc.0c00693
J. Chem. Theory Comput. 2020, 16, 7381−7399